

# Unleashing Efficient Asynchronous RL Post-Training via Staleness-Constrained Rollout Coordination

Haoyang Li<sup>\*1</sup>, Sheng Lin<sup>\*1</sup>, Fangcheng Fu<sup>2</sup>, Yuming Zhou<sup>1</sup>, Xiaodong Ji<sup>1</sup>, Yanfeng Zhao<sup>2</sup>, Lefeng Wang<sup>2</sup>, Jie Jiang<sup>3</sup>, Bin Cui<sup>1</sup>

<sup>1</sup>Peking University, <sup>2</sup>Shanghai Jiao Tong University, <sup>3</sup>Tencent Inc.

## Abstract

Reinforcement learning (RL) post-training has become pivotal for enhancing the capabilities of modern large models. A recent trend is to develop RL systems with a fully disaggregated architecture, which decouples the three RL phases (rollout, reward, and training) onto separate resources and executes them asynchronously. However, two critical data-level concerns arise: (1) asynchronous execution leads to *data staleness* in trajectories (the data generated by rollout) as the model parameters used in rollout may not be up to date, which impairs RL convergence; and (2) the length variation of trajectories introduces severe *data skewness*, leading to workload imbalance and degraded system performance.

Existing systems fail to address these two concerns in a unified manner. Techniques that tightly control data staleness often constrain effective data skewness mitigation, while aggressive data skewness mitigation tends to exacerbate data staleness. As a result, systems are forced to trade off convergence for performance, or vice versa. To address this, we propose STALEFLOW, an RL post-training system that jointly tackles data staleness and skewness. First, to control staleness, STALEFLOW introduces a global consistency protocol that tracks the full lifecycle of each trajectory and constrains staleness. Second, to mitigate skewness, STALEFLOW redesigns the RL system architecture by constructing data servers for trajectories and parameters to achieve flexible rollout coordination. Subsequently, we develop a suite of staleness-aware, throughput-oriented strategies to enhance system performance. Evaluations show that STALEFLOW achieves up to 1.42-2.68× (1.17-2.01× on average) higher throughput than state-of-the-art systems, without compromising convergence.

## 1 Introduction

With the diminishing returns from scaling large model pre-training, the research community has increasingly focused on scaling reinforcement learning (RL) during post-training as the next frontier for advancing model capabilities [25, 65]. Recently, we have witnessed the emergence of large models with deep reasoning capabilities (e.g., OpenAI-o1 [51], Kimi-K2 [66], DeepSeek-R1 [5]), many of which rely on RL to enable long-chain reasoning [53, 69, 85].

A common workflow of RL post-training consists of three phases: *rollout*, *reward*, and *training* [58, 59, 61, 82, 90]. A growing trend is to decouple these phases, deploy them on dedicated resources, and execute them asynchronously. Compared to shared-resource designs, such disaggregated architectures typically offer substantially better scalability [10, 15, 16, 41, 42, 48, 62, 76, 94].

<sup>\*</sup>Equal contribution

Contact: Haoyang Li (2000012918@stu.pku.edu.cn), Fangcheng Fu (cc-chengff@sjtu.edu.cn) and Bin Cui (bin.cui@pku.edu.cn)

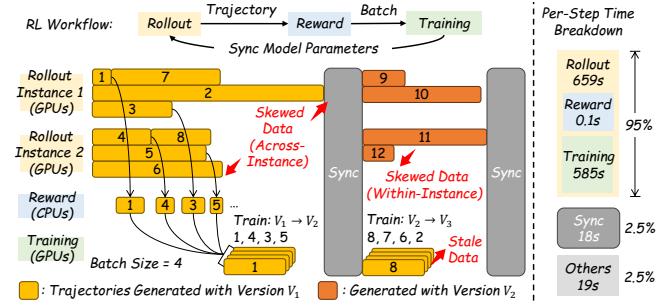


**Figure 1:** (Left) RL workflow in a fully disaggregated architecture. (Right) Time breakdown of post-training a Qwen3-30B-A3B (64 H20 GPUs). Rollout and training overlap and jointly dominate the time.

From the data management perspective, there are two kinds of data that move across different phases, namely *trajectories* and *parameters*. As illustrated in Figure 1, RL trajectories are generated in a streaming manner across multiple rollout instances (i.e., model replicas), and then forwarded to the reward stage upon completion. Once sufficient rewarded trajectories are accumulated to form a batch, the model is trained and updated. Finally, the model parameters are synchronized back to the rollout side, completing an RL post-training step. In this loop, rollout and training overlap and together dominate the end-to-end execution time.

**Concerns from data.** Within this asynchronous workflow, two fundamental data-level concerns arise. (1) **Data staleness.** Asynchronous execution of rollout and training significantly improves system throughput, but it also causes the training stage to consume stale trajectories, as the parameters used in rollout may not be up to date. Undoubtedly, this risks impaired convergence, as analyzed in §2.2. (2) **Data skewness.** During rollout, trajectory lengths vary substantially, leading to workload skewness both *within* an instance and *across* instances. This imbalance degrades resource utilization and overall system performance, as analyzed in §2.3.

To control data staleness, existing systems adopt different approaches, ranging from strong to weak guarantees: (1) Some systems [10, 41] allow users to specify an explicit *staleness bound*  $\eta$ , thereby strictly bounding staleness. (2) Other systems [15, 16, 42] do not support configurable bounds and only permit one-step asynchrony (i.e.,  $\eta = 1$ ). (3) The remaining systems [62, 76, 86, 96] provide no explicit staleness guarantees. To mitigate data skewness, various rollout coordination techniques have been proposed: (1) Partial rollout [6, 10, 15, 41, 67, 76], which allows a single trajectory to be generated by multiple model versions; (2) Redundant rollout [12, 86, 96], which oversamples trajectories and discards long-tail ones; (3) Rollout with multi-version instances [15, 16, 62],

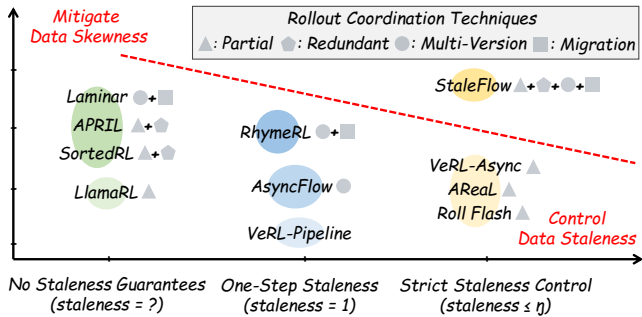


**Figure 2: Comparison of different RL systems.** Higher values on the vertical axis indicate stronger support for rollout coordination.

where instances update models at their own pace without global synchronization; and (4) Migration across instances [12, 16, 54, 62], which dynamically redistributes trajectories to rebalance workload.

**Limitations.** Despite these advances, current systems fall short in striking a good balance between staleness control and skewness mitigation, as shown in Figure 2. Designs that enforce strict staleness guarantees necessarily constrain skewness mitigation, as many rollout coordination techniques risk violating the *staleness bound*. In contrast, systems that support rich and flexible rollout coordination typically relax staleness control in favor of higher throughput. As a result, existing approaches are forced into a trade-off between RL convergence and system performance.

**Challenges and motivations.** This limitation arises from two unresolved challenges: (1) First, as rollout coordination techniques mostly operate on the trajectories, to synergize both worlds, a fine-grained, trajectory-level staleness control is expected, yet this is unexplored in current strict control approaches. (2) Second, existing systems lack a globally coordinated, staleness-aware rollout coordination framework to mitigate skewness: existing techniques are applied in isolation and ad hoc, without explicitly modeling and optimizing system throughput under a given *staleness bound*.

To address these challenges, we present STALEFLOW, an RL post-training system that jointly provides strong staleness guarantees and high system performance. (1) To control data staleness (§4), we propose a novel global consistency protocol built on a virtual staleness buffer abstraction, which tracks the lifecycle of each trajectory at fine granularity. This makes our system compatible with advanced rollout coordination techniques while enabling precise staleness control. (2) To mitigate data skewness and improve system performance (§5), we introduce innovations in both rollout architecture and algorithms. Architecturally, we introduce two middleware data servers (i.e., a trajectory server and a parameter server) to decouple data movement from rollout. This decoupling allows rollout instances to selectively determine when and how to fetch and coordinate data, substantially improving flexibility. Algorithmically, we develop a suite of staleness-aware, throughput-oriented rollout coordination strategies. These strategies are orchestrated by a centralized coordinator that continuously analyzes system snapshots and issues commands to actively steer system behavior.

In summary, our contributions are as follows:

- We propose a global consistency protocol that enforces strict staleness control at the trajectory level while supporting advanced rollout coordination techniques (§4).
- We introduce architectural innovations that decouple data movement into dedicated servers, serving as middleware to enable flexible rollout coordination (§5.1).
- We design a suite of staleness-aware, throughput-oriented rollout coordination strategies that unify diverse techniques to maximize system throughput under explicit staleness constraints, implemented via a snapshot-command cycle (§5.2, §5.3).
- Evaluations on a 128-GPU cluster show that STALEFLOW achieves  $1.42\text{-}2.68\times$  ( $1.17\text{-}2.01\times$  on average) throughput improvement over state-of-the-art RL systems, while preserving convergence (§6).

## 2 Preliminaries and Motivations

In this section, we explore the workflow of RL post-training and investigate two emerging data-level concerns. We then discuss existing solutions addressing these concerns and analyze their limitations, which ultimately motivate the design of our work.

### 2.1 RL Workflow and Trend

**RL workflow.** As illustrated in Figure 1, a typical RL post-training workflow consists of three distinct phases. (1) **Rollout phase.** The model samples prompts from a dataset and generates responses token-by-token through auto-regressive decoding. The prompt and its corresponding response are then concatenated to form an RL trajectory.<sup>1</sup> (2) **Reward phase.** The system applies rule-based or verifiable reward models [73, 83] to evaluate generated trajectories and assign scalar scores, which serve as reward signals. (3) **Training phase.** A selected RL algorithm consumes the collected trajectories and their reward, batches the data for model training, and synchronizes the updated parameters back to the rollout side.

**Fully disaggregated architecture.** The three RL phases exhibit distinct resource requirements and computational characteristics. Both the rollout and training phases rely on GPUs for acceleration, but they differ significantly in their nature: the rollout phase is memory-bound, performing token-by-token decoding, while the training phase is compute-bound, involving large-batch forward and backward passes, and scales more efficiently with additional GPUs. In contrast, the reward phase typically runs on CPUs, executing rule-based or verifiable evaluations. Given these differences, a key trend in RL system design is to *fully disaggregate the three phases* and allocate them to specialized resources [10, 15, 16, 41, 42, 48, 62, 76, 94]. As shown in Figure 1, unlike synchronous RL systems that rely on shared resources and sequential execution (e.g., VeRL [63]), this disaggregated architecture enables the phases to execute in an overlapped and asynchronous manner, allowing each phase to independently optimize its resource utilization and performance.

**Data-Level concerns.** However, such a disaggregated architecture faces two critical data-level concerns. (1) **Data staleness.** To enable overlapped and asynchronous execution of training and rollout, systems need to train on trajectories generated by older versions of the model. For example, as shown in Figure 1, training from version  $V_2$  to  $V_3$  consumes data generated by  $V_1$ , thereby allowing

<sup>1</sup>For clarity, a prompt alone is considered an *initial trajectory* in this paper.

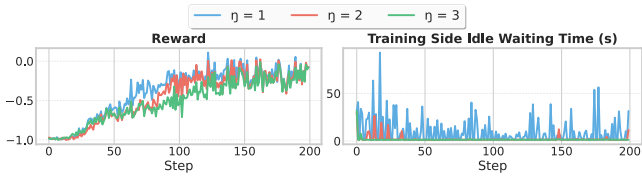


**Figure 3: Effect of staleness bounds ( $\eta$ ) on post-training Qwen2.5-MATH-7B with DAPO [82] (64 H20 GPUs). A larger staleness bound reduces idle waiting in training but slows convergence.**

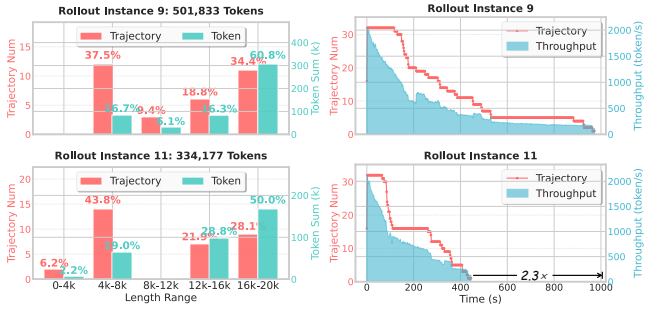


**Figure 4: A rollout step of Qwen3-30B-A3B (128 H20 GPUs). (Left) Trajectory and token distributions are highly skewed both *within* each instance and *across* different instances. (Right) This causes intra-instance underutilization and inter-instance idle waiting.**

the  $V_2$  training phase to overlap with the  $V_2$  rollout phase. While this improves resource utilization, it introduces stale data, which may impair RL convergence when the staleness becomes excessive. (2) **Data skewness.** During rollout, trajectory lengths may vary significantly. As shown in Figure 1, because trajectory generation is distributed across multiple rollout instances (i.e., model replicas), this skewness manifests both *within-instance* (uneven loads from long vs. short sequences within the same instance) and *across-instance* (different instances progressing at different speeds). Both forms of skewness degrade overall RL system performance.

In the following, we present a detailed analysis of data staleness and skewness in RL, exploring their root causes and impacts, and classify existing solutions based on how they address them.

## 2.2 Data Staleness in RL

**Root causes.** RL algorithms inherently tolerate a certain degree of model mismatch through importance sampling [7, 68]. Recent advances further prove that, by applying additional corrections to importance weights [6, 10, 39, 80, 87, 89, 91], RL post-training can maintain stability under model mismatch even at a large scale. This allows rollout to use models that deviate from those used in training. For example, rollout may adopt low-precision quantization (e.g., FP8) [21, 40], or be executed on specialized inference stacks that exhibit inherent precision discrepancies compared to training [39, 80, 87, 89]. More critically, rollout can be performed using historical or mixed model versions, enabling concurrent training on older

trajectories while new ones are still being generated [6, 10, 89, 91]. As shown in Figure 1, this introduces stale data.

**Impacts.** In practice, to prevent excessive model discrepancy, RL post-training could typically impose a global *staleness bound*  $\eta$ , restricting training to data that is at most  $\eta$  model versions old. As illustrated in Figure 3, increasing  $\eta$  generally degrades convergence, as the rollout model diverges more from the training model. However, tolerating higher staleness can substantially improve system throughput by allowing more rollout trajectories to proceed concurrently and reducing idle waiting times on the training side.

**Current solutions.** Existing solutions can be broadly classified into three categories based on how they regulate or tolerate staleness.

(1) **Strict staleness control.** The first category, exemplified by VeRL-Async [17], AReAL [10], and ROLL Flash [41], grants users full autonomy in selecting  $\eta$ . They enforce strict staleness control through global safeguards. Specifically, they limit the total amount of in-flight data (i.e., trajectories that are either being generated or have been generated but not yet consumed) to  $(\eta + 1) \times \text{batch\_size}$ . Once this limit is reached, further rollout generation is halted.

(2) **One-Step staleness.** The second category includes systems such as VeRL-Pipeline [18, 42], AsyncFlow [15], and RhymeRL [16]. These systems do not support user-defined *staleness bounds* and only permit one-step asynchrony (i.e.,  $\eta = 1$ ). During training, they strictly use a model that is at most one version behind to generate exactly one batch, ensuring that staleness never exceeds one step.

(3) **No staleness guarantees.** The third category consists of systems such as LlamaRL [76], Laminar [62], APRIL [96], and Sort-erDRL [86]. These systems do not introduce explicit mechanisms to control or bound data staleness during execution, allowing rollout and training to proceed fully asynchronously without constraints.

## 2.3 Data Skewness in RL

**Root causes.** Data staleness arises from model version mismatches during asynchronous rollout generation and training. In contrast, data skewness is inherent to RL execution. As shown in Figure 4 (left), due to the auto-regressive nature of large models, trajectories vary in length. In large-scale RL post-training (e.g., GRPO [61]), which often follows an ORM paradigm [5, 35], only complete trajectories can be rewarded and used for training. Thus, training must wait for the longest trajectory in a batch. This behavior gives rise to the data skewness issue that limits the overall system performance.

**Impacts.** As illustrated in Figure 4 (right), data skewness manifests in two forms. First, *within an instance*, shorter trajectories finish quickly, leaving the instance occupied for a prolonged period by a small number of long-tail trajectories, thus keeping throughput low. Second, *across instances*, some instances finish much faster than others; faster instances therefore must wait for the slowest one before the system can synchronize model parameters globally. Both types of skewness constrain the overall system throughput.

**Current solutions.** To mitigate these issues, several rollout coordination techniques have been proposed, as summarized in Figure 5.

(1) **Partial rollout trajectories** [6, 10, 15, 41, 67, 76]. As noted in §2.2, training can proceed on trajectories collected from mixed historical model versions. Therefore, model synchronization can occur while rollout is still in progress. As shown in Figure 5(a), we can

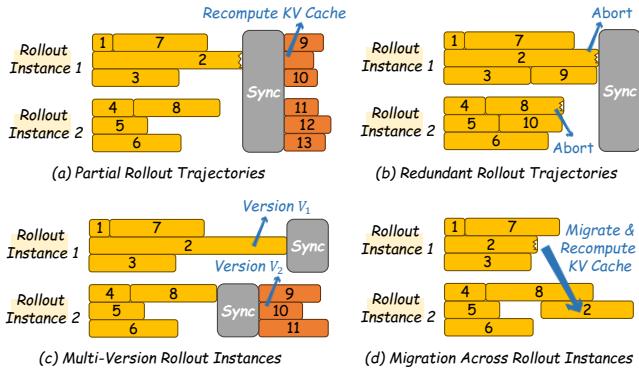


Figure 5: Rollout coordination techniques for mitigating skewness.

interrupt an ongoing trajectory, synchronize the model, recompute the KV Cache (i.e., re-prefill), and then resume generation. This allows the instance to promptly admit data from newer versions (e.g., trajectories 9 and 10), thereby alleviating *within-instance* skewness.

(2) **Redundant rollout trajectories** [12, 86, 96]. Another technique is to oversubscribe the number of trajectories. For example, in Figure 5(b), once the required number of trajectories (e.g., 8) have been generated, the remaining ones (e.g., trajectories 2 and 8) can be aborted. This naturally filters out long-tail trajectories and mitigates *within-instance* skewness.

(3) **Multi-Version rollout instances** [15, 16, 62]. While the methods above alleviate *within-instance* skewness, faster instances may still be blocked by slower ones. To address this, as shown in Figure 5(c), different instances can independently synchronize the model. Instances running at different speeds may thus generate trajectories using different model versions, eliminating the need for global synchronization and reducing *across-instance* skewness.

(4) **Migration across rollout instances** [12, 16, 54, 62]. A further technique involves migrating trajectories across rollout instances. As illustrated in Figure 5(d), a running trajectory (e.g., trajectory 2) can be interrupted and migrated to another instance, where it is re-prefilled and generation resumes. This approach mitigates both *within-instance* skewness (by migrating long-tail trajectories) and *across-instance* skewness (by balancing load across faster and slower instances).

## 2.4 Limitations, Challenges, and Motivations

Despite these optimizations proposed to address staleness and skewness, existing systems share a key limitation: they fail to jointly control staleness and mitigate skewness, as shown in Figure 2.

(1) **Systems with strict staleness control** typically bound staleness by limiting the amount of in-flight data. This design is overly restrictive, as it assumes a single model version on the rollout side and fixed trajectory assignment. As a result, such systems cannot support rollout with multi-version instances, redundant rollout, or flexible migration across instances, since these rollout coordination techniques may violate the prescribed staleness constraints. Consequently, their ability to mitigate data skewness is constrained.

(2) **Systems with one-step staleness** ensure that the version gap

between rollout and training is at most one. This guarantee enables more flexible rollout coordination, such as rollout migration or allowing faster instances to synchronize model parameters early. However, their staleness bound is fixed to one (i.e.,  $\eta = 1$ ) and cannot be increased for further performance gains. (3) **Systems without staleness guarantees** impose no constraints on staleness and freely apply rollout coordination, which enables high system throughput. However, the lack of staleness control can result in unbounded staleness, potentially harming convergence.

In summary, existing systems struggle to jointly balance data staleness control and data skewness mitigation. Approaches that aggressively mitigate data skewness tend to weaken staleness control, while enforcing strict staleness guarantees constrains rollout coordination flexibility, making skewness difficult to handle. Therefore, current solutions often sacrifice either convergence stability or system performance. This exposes a core question: *how can a system simultaneously enforce bounded data staleness for convergence and mitigate data skewness to maximize performance?* Addressing this question entails two fundamental challenges.

(C1) **Rigorous enforcement of bounded staleness.** Existing systems control data staleness using coarse-grained mechanisms that limit in-flight data, which are inflexible and narrow in scope. A more general and systematic staleness control mechanism is needed to support diverse rollout coordination techniques while ensuring that predefined staleness bounds are preserved.

(C2) **Unified mitigation of data skewness under staleness bounds.** Existing systems mitigate data skewness by selectively applying individual rollout coordination techniques, without globally coordinating their interactions or accounting for their combined effects given a *staleness bound*. A unified system design with globally coordinated, staleness-aware rollout coordination strategies is needed to enable more effective skewness mitigation.

To address these challenges, we present STALEFLOW. To tackle (C1), STALEFLOW introduces a novel consistency protocol based on the virtual staleness buffer abstraction, which ensures that all rollout coordination preserves the specified *staleness bound* via buffer-based primitives: Reserve, Occupy, and Consume (§4). To address (C2), STALEFLOW incorporates two additional data servers (i.e., a trajectory server and a parameter server), enabling flexible rollout coordination. Furthermore, it encapsulates various rollout coordination techniques into a set of rollout commands and employs staleness-aware, throughput-oriented strategies driven by real-time snapshots (§5). Together, these designs enable STALEFLOW to mitigate data skewness in a unified manner, maximizing system performance while preserving strict staleness guarantees.

## 3 Overview

In this section, we present the overall design and system overview of STALEFLOW, along with its end-to-end data flow. As shown in Figure 6, our system comprises four major components: a staleness manager, a rollout service with a centralized coordinator, a reward server, and training workers. Particularly, the first two components are novelly designed in our system.

To control data staleness (§4), we introduce the staleness manager that enforces a global consistency protocol, continuously interacting with all system components to ensure that no operation

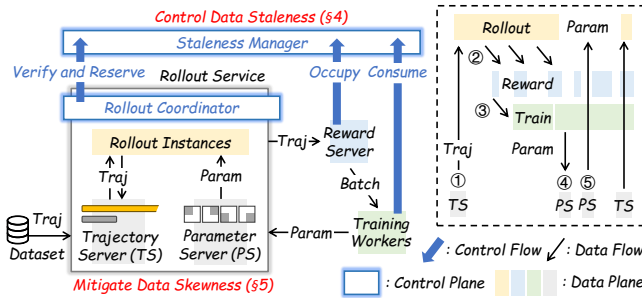


**Figure 6: (Left)** Overview of STALEFLOW. A staleness manager enforces strict data staleness control, while a rollout coordinator and two data servers provide flexible, efficient rollout coordination to mitigate data skewness. **(Right)** Standard data flow in STALEFLOW. Trajectories are sourced from the TS (1) and flow through the rollout, reward, and training phases (2–3). After training a batch, updated model parameters are pushed to the PS (4), and rollout instances selectively pull fresh parameters as needed (5).

violates the predefined *staleness bound*. Specifically, (1) The rollout coordinator first consults the staleness manager to verify whether generating a trajectory on a given rollout instance would violate the *staleness bound*. If admitted, rollout generation starts, and the protocol performs Reserve to mark the trajectory as in progress. (2) Upon completion of the rollout and reward computation, the protocol performs Occupy to register the trajectory as ready for consumption. (3) Once a full training batch is accumulated, the training workers invoke Consume to retire the batch. Through these interactions, the protocol explicitly tracks the lifecycle of each trajectory and guarantees strict adherence to the global staleness constraint.

To mitigate data skewness (§5), we further augment the rollout service with two dedicated data servers: a trajectory server (TS) and a parameter server (PS). The TS manages all trajectories involved in rollout generation and mediates access between the dataset and the rollout instances, while the PS maintains the latest model parameters and provides a synchronization interface between the training workers and the rollout instances. As shown in Figure 6 (right), these servers operate as middleware that continuously supply fresh trajectories and up-to-date model parameters for rollout. The key intuition is that, by decoupling the data movement (trajectories and model parameters) from the rollout instances, STALEFLOW gains fine-grained control over when and where trajectories should be routed and model parameters should be synchronized. Together governed by a centralized coordinator, the rollout service thus achieves flexible and efficient rollout coordination.

## 4 Control Data Staleness

This section presents how the staleness manager enforces a strict *staleness bound*  $\eta$  via a global consistency protocol built around trajectory version identifiers (§4.1). The protocol is realized through a set of buffer-based primitives: Reserve, Occupy, and Consume (§4.2), and is designed to remain compatible with a wide range of advanced rollout coordination techniques (§4.3).

### 4.1 Trajectory Version Identifier

Enabling flexible rollout coordination requires the ability to track data and bound staleness at the trajectory level. To achieve this, each initial trajectory in STALEFLOW is assigned a version identifier, denoted as  $V_{traj}$ , which indicates the model version that will be used to generate the trajectory. If partial rollout is enabled (i.e., different segments may be generated using different versions), it refers to the oldest tolerated version. The assignment of  $V_{traj}$  is handled jointly by the rollout coordinator and the staleness manager.

The rollout coordinator dynamically proposes  $V_{traj}$  for initial trajectories before generation. The staleness manager, on the other hand, serves a dual role as both a discriminator and a tracker. (1) *As a discriminator*, it verifies whether a proposed  $V_{traj}$  would violate the specified *staleness bound*  $\eta$ . If not, the rollout coordinator may proceed to assign this  $V_{traj}$ . (2) *As a tracker*, it persistently records  $V_{traj}$  once assigned and maintains the lifecycle of each trajectory.

Through these two functions, the staleness manager ensures that all trajectories are assigned a  $V_{traj}$ , are properly tracked, and strictly adhere to the global staleness constraint.

### 4.2 Global Consistency Protocol

**Staleness buffer.** Within the staleness manager, we introduce the virtual staleness buffer abstraction, which serves as the core protocol for recording  $V_{traj}$ , tracking trajectories, and bounding staleness. As shown in Figure 7 (left), each buffer has a capacity equal to the batch size and stores an entry for each trajectory, maintaining its metadata: the ID and its  $V_{traj}$ . A buffer itself also holds a buffer version  $V_{buf}$ , meaning that trajectories inside this buffer will be used for training as the model advances from version  $V_{buf}$  to  $V_{buf} + 1$ . The staleness bound  $\eta$  is therefore enforced by requiring that any trajectory in any buffer satisfy the constraint:  $V_{traj} + \eta \geq V_{buf}$ .

During execution, while the rollout service and reward server act as producers and fill buffers with trajectories, the training workers continuously Consume staleness buffers to train the model.

**As a tracker.** The protocol tracks the lifecycle of a trajectory using two primitives: (1) Reserve, which places a temporary entry as a placeholder for a trajectory that has started but not yet completed; and (2) Occupy, which finalizes and records a completed, rewarded trajectory in the buffer. To make full use of the bound  $\eta$ , the protocol adopts a worst-case Reserve and greedy Occupy mechanism.

As shown in Figure 7 (left) at  $T_1$ , when a trajectory with  $V_{traj}$  begins execution and triggers a Reserve, the protocol performs a backward scan across buffers from  $V_{buf} = V_{traj} + \eta$  (the latest buffer where it may still safely train) down to  $V_{buf} = V_{traj}$ , reserving the latest available empty entry. This reflects the worst-case buffer position where the trajectory could reside without violating  $\eta$ .

As shown in Figure 7 (left) at  $T'_1$ , once rollout completes and reward is computed, the reserved entry is deleted and Occupy is triggered. Unlike worst-case backward reservation, Occupy scans forward and greedily occupies the earliest available empty entry. This design maximizes buffer utilization and admits the largest possible number of trajectories under the bound  $\eta$ .

**As a discriminator.** When the rollout coordinator consults the protocol to verify whether a particular  $V_{traj}$  can be assigned, the protocol only needs to simulate a Reserve: If an empty entry can

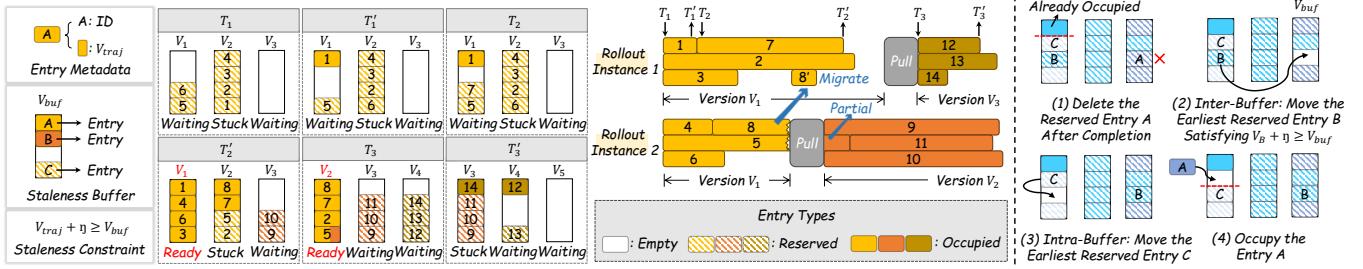


Figure 7: (Left) Staleness buffers enforce the bound  $\eta$  using Reserve and Occupy. For illustration, Occupy is drawn immediately after rollout completion; in practice, it occurs after reward computation. In this example,  $\eta = 1$  (i.e.,  $V_{traj} + 1 \geq V_{buf}$ ), and each rollout instance supports up to three concurrent trajectories. (Right) Buffer transitions when a Reserve completes and a corresponding Occupy must be applied.

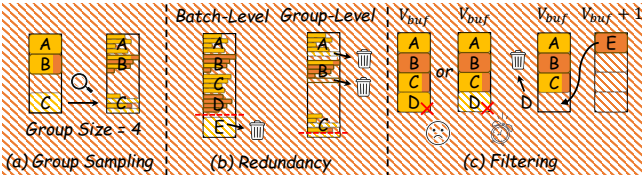


Figure 8: The staleness buffer is designed to be fully compatible with a wide range of advanced rollout coordination techniques.

still be successfully claimed, the assignment is permitted. Otherwise, a larger  $V_{traj}$  is needed to unlock newer buffers for reservation, guaranteeing that the *staleness bound*  $\eta$  remains satisfied.

**Buffer states.** As illustrated in Figure 7 (left), a staleness buffer can be in one of three states: (1) *Waiting*. The buffer still contains empty entries and Reserve may continue. For example, at  $T_2$ , buffers with  $V_{buf} = V_1$  through  $V_{buf} = V_2$  remain in the *Waiting* state, allowing trajectory 7 to continue being assigned  $V_{traj} = V_1$  and routed to instance 1. (2) *Ready*. All entries are occupied, allowing the buffer to be consumed by training. (3) *Stuck*. The buffer is full but contains at least one reserved (unfinished) entry. In this state, training and further reservations are blocked until the in-flight trajectories are complete. For example, at time  $T_2'$ , buffer  $V_{buf} = V_2$  is *Stuck*, preventing additional trajectories from being routed to instance 1 with  $V_{traj} = V_1$ , whereas buffer  $V_{buf} = V_3$  is not *Stuck*, allowing trajectories to be assigned  $V_{traj} = V_2$  and routed to instance 2.

**Entry deletion and movement.** Before a completed trajectory can be occupied, its reserved entry must be deleted. This deletion may trigger movement of other reserved entries to ensure that Occupy can occur as early as possible. Figure 7 (right) illustrates the procedure: (1) Let a reserved entry A with version  $V_A$  be located in buffer  $V_{buf}$  and be ready for deletion. (2) We scan buffers from smallest up to  $V_{buf}$  to find the earliest reserved entry B satisfying  $V_B + \eta \geq V_{buf}$ , and move B to A's position. (3) If B's original buffer then exposes a smaller reserved entry C, C is moved into B's former position. (4) Finally, Occupy is executed for trajectory A at the earliest empty entry. This transition keeps ready-to-use (occupied) entries in earlier buffers while pushing reserved entries toward later buffers, maintaining maximal readiness for training.

**Discussions.** This global consistency protocol is lightweight, as it only needs to record the metadata of trajectories (ID and  $V_{traj}$ ) without storing the actual payload. Furthermore, the total amount of data it needs to track corresponds to the amount of in-flight data (after Consume, data is no longer tracked), which is at most  $(\eta + 1) \times \text{batch\_size}$ . This depends solely on the configuration of the RL algorithm and is independent of the cluster scale.

### 4.3 Compatibility with Advanced Techniques

**Partial rollout and rollout migration.** As illustrated in Figure 7 (left), the protocol naturally supports both partial rollout and rollout migration. The key reason is that the  $V_{traj}$  stored in each buffer entry represents the oldest model version tolerated over the entire trajectory generation process (see §4.1). This value is agnostic to how individual segments are produced—whether different segments are generated using different model versions (partial rollout) or by different rollout instances (rollout migration). As a result, changes in the underlying model version or execution instance across segments do not alter the buffer state. For example, in Figure 7 (left), trajectory 5 undergoes partial rollout at time  $T_2'$ . However, this internal change is transparent to the protocol, and the reserved entry for trajectory 5 in buffer  $V_{buf} = V_2$  remains unchanged.

**Group sampling.** RL algorithms may specify a group size alongside the batch size to generate multiple trajectories for the same prompt and process them as a whole [61, 82, 90]. As shown in Figure 8(a), in such cases, we maintain buffer entries at the granularity of trajectory groups and perform Reserve/Occupy per group. A reserved entry can be deleted and occupied only when all trajectories in the group are complete (e.g., entry C in the figure remains reserved because two trajectories in its group are still unfinished). Besides, the version recorded for the group is the minimum  $V_{traj}$  across all trajectories in the group  $\mathcal{G}$ , i.e.,  $\min_{traj \in \mathcal{G}} \{V_{traj}\}$ , indicating the maximum staleness tolerated for the whole group.

**Redundancy and filtering.** The staleness buffer also accommodates flexible redundant rollout and rollout filtering. (1) As shown in Figure 8(b), redundancy can be applied at either the batch level (expanding the number of buffer entries) or the group level (increasing the number of trajectories per entry). When a buffer reaches its predefined batch size or an entry reaches its group size, surplus data can be aborted, dropping trajectories that take too long to generate.

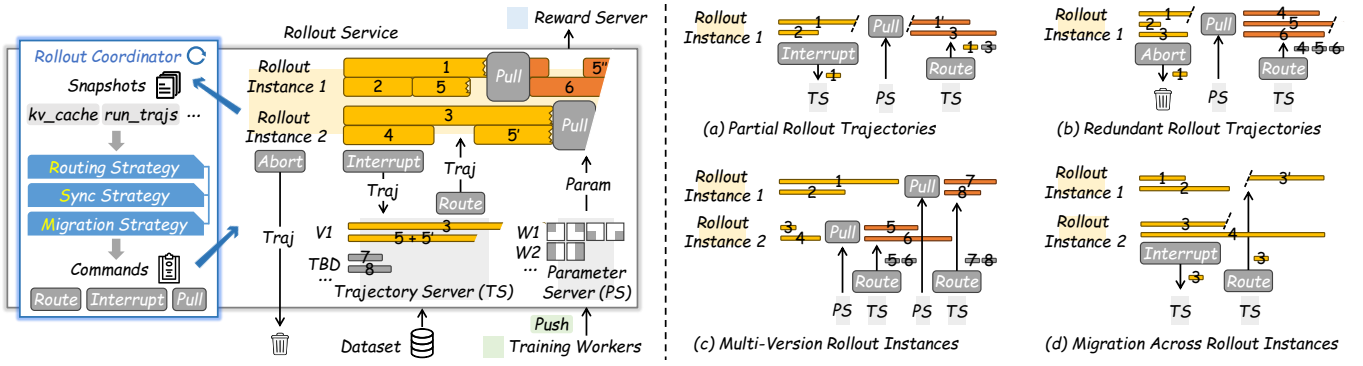


**Figure 9: (Left)** Rollout service architecture. The centralized coordinator periodically captures snapshots and issues commands to coordinate rollout instances, TS, and PS. **(Right)** Diverse rollout coordination techniques are supported via different commands based on TS and PS.

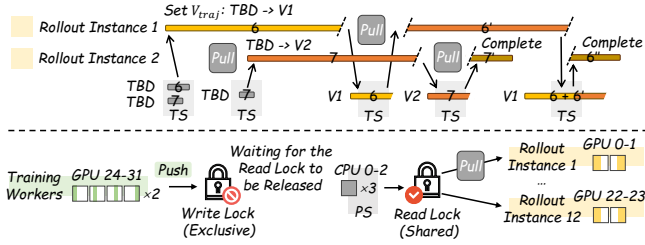


**Figure 10: Decoupling rollout data movement (trajectories and model parameters) via middleware servers. (Top)** TS: Trajectories flow through different rollout instances via the TS as an intermediary. **(Bottom)** PS: Training workers continuously Push updated model parameters to the PS, while rollout instances Pull them on demand. A read-write locking scheme is used to ensure correctness.

(2) As shown in Figure 8(c), while redundancy results in passive abortion, we can also proactively filter certain occupied or reserved entries, e.g., when trajectories are not needed by the algorithm (e.g., identical rewards within a group provide no learning signal [82]) or when training is stalled waiting for excessively delayed trajectories. After abortion, occupied entries from later buffers can be moved forward to fill the empty slot, allowing the buffer to become *Ready* quickly without waiting for new trajectories to complete.

## 5 Mitigate Data Skewness

While data staleness is rigorously enforced by the global staleness manager, data skewness is handled within the rollout service through a centralized coordinator and two dedicated data servers (§5.1). The coordinator continuously executes a snapshot-command cycle (§5.2) to deploy a suite of rollout coordination strategies (§5.3), which mitigate data skewness and enhance system performance.

### 5.1 Rollout Service Architecture

**Design intuitions.** Most existing RL systems manage data movement in a closed-loop manner, where trajectories are fed directly

from datasets to rollout instances, and model parameters are synchronized directly from training workers to rollout instances. While straightforward, this tight coupling makes coordination on rollout instances challenging: trajectories may require interruption, resumption, or migration across instances, and breaking the global synchronization necessitates instances to update models independently. To address this, we introduce a trajectory server (TS) and a parameter server (PS) that serve as middleware storage, thereby decoupling the data movement. As illustrated in Figure 9 (left), with the rollout coordinator acting as the central control plane, we can flexibly coordinate rollout instances through the support of TS and PS, enabling controlled delivery of trajectories and parameters.

**Rollout coordinator.** As shown in Figure 9 (left), the coordinator periodically captures snapshots of rollout instances, applies a suite of rollout coordination strategies based on them, and subsequently issues rollout commands. These commands include (1) Pull, which instructs a designated rollout instance to fetch the latest model parameters from the PS; (2) Route, which selects a trajectory from the TS and assigns it to a specific rollout instance for generation; and (3) Interrupt, which terminates an ongoing trajectory on a given instance and returns the partially generated trajectory to the TS.<sup>2</sup> As shown in Figure 9 (right), by composing these commands and leveraging the TS and PS as middleware, rollout instances can realize a wide range of rollout coordination techniques.

**Trajectory server.** The TS stores all trajectories required by the rollout instances, with a default capacity of  $(\eta + 1) \times \text{batch\_size}$ . It continuously samples prompts from the dataset, processes them, and enqueues them as initial trajectories within the capacity limit. As shown in Figure 10 (top), these initial trajectories are not yet assigned a  $V_{traj}$  (see §4.1), which is done during routing. At that time, the rollout coordinator consults the staleness manager to verify admissible version candidates (see §4.2), assigns an appropriate  $V_{traj}$ , and selects a target rollout instance according to the *routing strategy* (§5.3). If a trajectory is interrupted during generation, it is returned to the TS and re-routed later. The *routing strategy* ensures that for such partially generated trajectories, the model version of

<sup>2</sup>In addition, the staleness manager may directly issue Abort commands to rollout instances to irrevocably discard a trajectory, as discussed in §4.3. In this case, the trajectory will not be returned to the TS.

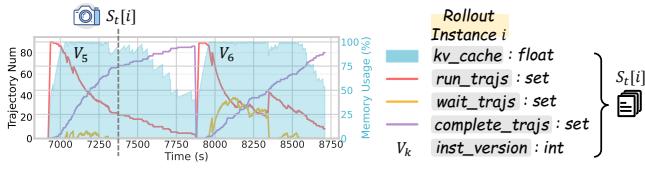


Figure 11: A snapshot captures five fields for every rollout instance.

the re-routed rollout instance is no older than the assigned  $V_{traj}$ , as it represents the oldest version tolerated over the entire generation.

**Parameter server.** The PS stores the latest model parameters and, as shown in Figure 10 (bottom), is deployed with multiple workers to support distributed storage over CPU resources. During execution, the rollout coordinator issues Pull commands according to the *synchronization strategy* (§5.3), directing specific rollout instances to retrieve parameters from the PS. Conversely, model updates on the PS are made via Push operations, triggered automatically by the training workers. Once a training step completes, the training workers immediately Push the updated parameters to the PS, overlapping the communication with the next training step. Additional implementation and resource deployment details, along with communication optimizations, are provided in Appendix A.

To ensure correctness, the PS adopts a read-write locking scheme inspired by database concurrency control: A Push operation (analogous to an exclusive write) blocks concurrent Pull commands, and vice versa, while multiple Pull commands from different rollout instances (analogous to shared reads) may proceed concurrently.

**Discussions.** While introducing the TS and PS as middleware adds extra data movement from the dataset and training workers, the impact is minimal: reading pure tokens from the dataset imposes a light load, and the training workers’ Push operations can be overlapped. Moreover, as the cluster scales, the overhead of the TS does not grow due to its fixed capacity, while the Push and Pull for the PS also remain constant (see Appendix A.3). Our design therefore does not affect scalability. The time breakdown in §6.5 further demonstrates that the overhead of the TS, PS, and rollout coordination stays below 3% of the total time, confirming its efficiency.

## 5.2 Snapshot-Command Cycle

To mitigate data skewness, the rollout coordinator operates continuously in a snapshot-command cycle, monitoring the system’s real-time load and performing rollout coordination strategies.

**Fields of the snapshot.** Each captured snapshot  $S$  aggregates five fields for every instance: the GPU memory usage of the KV Cache (kv\_cache), the trajectories currently under generation (run\_trajs), the trajectories queued in the rollout engine’s internal waiting queue (wait\_trajs), the trajectories completed on the instance since the last model synchronization (complete\_trajs), and the instance’s current model version (inst\_version). As illustrated in Figure 11, during rollout, run\_trajs generally decreases while complete\_trajs monotonically increases. As trajectories grow longer, kv\_cache increases accordingly. Once it reaches the budget, trajectories from run\_trajs are preempted and moved into wait\_trajs, until kv\_cache is released. During parameter synchronization, all run\_trajs and

Table 1: Command arguments and their effects on the speculative state ( $P$ ). We denote “inst” as the targeted instance ID, “trajs” as the set of trajectory IDs to manipulate, and  $|\cdot|$  as set cardinality.

Commands	Arguments	Effects on $P$ After Issuance
Pull	inst	$P[\text{inst}].\text{inst\_version} = \text{get\_ps\_version}()$ $P[\text{inst}].\text{accum\_traj\_num} = 0$
Route	inst, trajs	$P[\text{inst}].\text{accum\_traj\_num} +=  \text{trajs} $
Interrupt	inst, trajs	$P[\text{inst}].\text{accum\_traj\_num} -=  \text{trajs} $
Abort	inst, trajs	$P[\text{inst}].\text{accum\_traj\_num} -=  \text{trajs} $

wait\_trajs are interrupted and cleared, and inst\_version is updated to reflect the newly synchronized model.

**Snapshot validation using speculative state.** Within this cycle of periodic snapshots, decision-making, and command execution, a key challenge arises from the temporal coupling between decisions and system state changes. As illustrated in Figure 12(a), when the rollout coordinator makes decisions and issues commands based on the snapshot  $S_t$ , these commands require a duration  $\Delta t$  to take effect in the real system after issuance. If  $S_{t+1}$  is captured before the effect of the commands is realized, it may reflect the system state prior to the command execution. Using such snapshots for subsequent decisions risks operating on outdated information, potentially leading to decision inconsistencies or oscillatory behavior.

Since  $\Delta t$  is highly variable and context-dependent, we introduce a snapshot validation mechanism centered on a *speculative state*  $P$ . It represents the expected system state after each issued command has fully taken effect, with two critical fields: the expected model version of each instance (inst\_version) and the expected accumulated number of trajectories (accum\_traj\_num) for each instance, including completed ones. At system startup, for every instance, both fields in  $P$  are initialized to 0. As summarized in Table 1, after each command is issued,  $P$  is updated correspondingly to reflect the expected effects of that command. Upon the arrival of a new snapshot  $S_{t+1}$ , the rollout coordinator validates it by checking, for every instance  $i$ , whether the following condition holds:

$$P[i].\text{inst\_version} = S_{t+1}[i].\text{inst\_version} \wedge P[i].\text{accum\_traj\_num} = |S_{t+1}[i].\text{run\_trajs} \cup S_{t+1}[i].\text{wait\_trajs} \cup S_{t+1}[i].\text{complete\_trajs}|. \quad (1)$$

A snapshot is accepted only if the condition is satisfied, indicating that all previously issued commands have taken effect; otherwise, it is discarded and the coordinator waits for the next snapshot.

**Concurrent command execution.** As shown in Figure 12(b), to maximize resource utilization, commands across different data planes are executed concurrently. However, this concurrency introduces cross-command dependencies. For example, a Route command must wait until all interrupted trajectories have been returned to the TS. Likewise, trajectories newly routed to an instance may be delayed if that instance is currently executing a Pull command to update its model. To preserve execution correctness in these cases, we enforce logical ordering by either having commands wait or by keeping the data pending in the relevant data planes, thereby excluding them from execution until the dependencies are resolved.

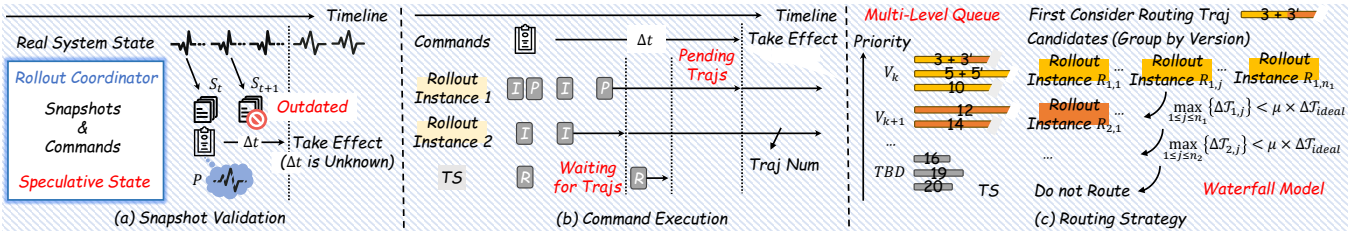


Figure 12: (a) To avoid outdated snapshots, we introduce a *speculative state* ( $P$ ) to verify whether the expected effect has occurred after issuing the commands. (b) After issuance, commands are executed concurrently. When dependencies exist between commands, we address them by either having commands wait or keeping data pending. “I”, “R” and “P” represent Interrupt, Route and Pull, respectively. (c) Our *routing strategy* utilizes a multi-level queue (MLQ) and a waterfall model to greedily optimize the marginal throughput benefits.

**Algorithm 1:** Rollout coordination procedure (detailed pseudocode for each strategy is given in Appendix D).

```

Input:  $S$ : the snapshot of all rollout instances (already validated)
1  $ts\_trajs \leftarrow get\_ts\_trajs();$ 
2  $ps\_version \leftarrow get\_ps\_version();$ 
3 foreach  $inst \in SynchronizationStrategy(S, ts\_trajs, ps\_version)$  do
4    $trajs \leftarrow S[inst].run\_trajs \cup S[inst].wait\_trajs;$ 
5    $ISSUECOMMAND(Interrupt(inst, trajs), Pull(inst));$ 
6    $S[inst].discard(trajs);$ 
7    $S[inst].inst\_version \leftarrow ps\_version;$ 
8    $ts\_trajs \leftarrow ts\_trajs \cup trajs;$ 
9 foreach  $(inst, trajs) \in MigrationStrategy(S)$  do
10   $ISSUECOMMAND(Interrupt(inst, trajs));$ 
11   $S[inst].discard(trajs);$ 
12   $ts\_trajs \leftarrow ts\_trajs \cup trajs;$ 
13 foreach  $(inst, trajs) \in RoutingStrategy(S, ts\_trajs)$  do
14   $ISSUECOMMAND(Route(inst, trajs));$ 

```

### 5.3 Rollout Coordination Strategies

A suite of staleness-aware, throughput-oriented rollout coordination strategies governs the decision-making process. As shown in Algorithm 1, given a system snapshot, these strategies are applied sequentially; each produces a set of commands that are issued asynchronously to steer system behavior. Due to space constraints, we outline only the core ideas of each strategy below; detailed pseudocode is provided in Appendix D.

**Cost model.** We first develop a cost model to estimate the throughput induced by a routing decision. Given a snapshot  $S$ , the generation throughput of instance  $i$ , denoted by  $\mathcal{T}_i$ , can be estimated as follows (the detailed derivation is provided in Appendix B):

$$\mathcal{T}_i(S) = \frac{|S[i].run\_trajs|}{k_1 \times S[i].kv\_cache + \max(k_2, k_3 \times |S[i].run\_trajs|) + k_4}. \quad (2)$$

Here,  $|\cdot|$  denotes set cardinality and  $k_1 \sim k_4$  are constant coefficients obtained via offline profiling and linear regression. Based on this cost model, we further derive the marginal throughput gain  $\Delta\mathcal{T}_i$

when routing a trajectory  $\tau$  of length  $l$  to instance  $i$ :

$$\begin{aligned}
y_i &= \mathbb{I}(S[i].kv\_cache + k_5 \times l \leq M \wedge |S[i].wait\_trajs| = 0). \\
S'[i].kv\_cache &= S[i].kv\_cache + y_i \times k_5 \times l. \\
S'[i].run\_trajs &= S[i].run\_trajs \cup \{\tau \mid y_i = 1\}. \\
S'[i].wait\_trajs &= S[i].wait\_trajs \cup \{\tau \mid y_i = 0\}. \\
\implies \Delta\mathcal{T}_i &= \mathcal{T}_i(S') - \mathcal{T}_i(S).
\end{aligned} \quad (3)$$

In this expression,  $\mathbb{I}(\cdot)$  is the indicator function,  $k_5$  denotes the per-token KV Cache footprint obtained via profiling, and  $M$  is the KV Cache budget. A routed trajectory  $\tau$  can run immediately (i.e.,  $y_i = 1$ ) only if it fits within the KV Cache budget and the rollout engine’s internal waiting queue is empty. Otherwise, it is placed into the waiting queue and contributes no throughput gain.

**Routing strategy.** Using the above cost model, we address how to route trajectories stored in  $TS$  under a given snapshot  $S$  (Algorithm 1, line 13). As shown in Figure 12(c), trajectories are first organized into a multi-level queue (MLQ) structure [57, 74] ordered by increasing  $V_{traj}$ . Smaller  $V_{traj}$  indicates higher staleness and thus higher routing priority, while initial trajectories without  $V_{traj}$  are assigned the lowest priority. This ordering reflects the principle that trajectories already identified as staler should be processed earlier. Accordingly, the routing procedure proceeds from the highest-priority non-empty queue; lower-priority queues are only considered once all higher-priority ones have been exhausted.

For a trajectory of length  $l$ , we first identify all candidate instances where routing is admissible. An instance  $i$  qualifies if either:

- The trajectory is initial, and the staleness manager permits assigning  $V_{traj} = S[i].inst\_version$  without violating  $\eta$  (§4.2).
- The trajectory already has a  $V_{traj}$ , indicating it is partially generated and interrupted, requiring re-routing. In this case, the re-routed instance must satisfy  $S[i].inst\_version \geq V_{traj}$ .

These candidate instances are then grouped by increasing  $inst\_version$ , yielding  $\{\{R_{i,j}\}_{j=1}^{n_i}\}_{i=1}^m$ . For one thing, instances with a smaller version should be prioritized, as they admit fewer feasible routing options. For another, we aim to maximize throughput by selecting the instance with the largest marginal throughput gain.

To balance priority and throughput, we leverage a simplified waterfall model [14, 26]. We define  $\Delta\mathcal{T}_{ideal}$ , which denotes the marginal throughput gain achieved by routing the trajectory to an idle

instance, serving as an upper bound on the achievable gain:

$$\Delta\mathcal{T}_{ideal} = \frac{1}{k_1 \times (0 + k_5 \times I) + \max(k_2, k_3 \times 1) + k_4} - 0. \quad (4)$$

As shown in Figure 12(c), starting from the highest-priority instance group, the algorithm selects the instance with the largest estimated gain  $\max_{1 \leq j \leq n_1} \{\Delta\mathcal{T}_{1,j}\}$ . If this gain exceeds the threshold  $\mu \times \Delta\mathcal{T}_{ideal}$ , the trajectory is routed to that instance; otherwise, the algorithm proceeds to the next group (i.e.,  $\{R_{2,1}, \dots, R_{2,n_2}\}$ ) and repeats the process. If no candidate instance yields a marginal gain exceeding the threshold, the trajectory is temporarily withheld from routing, allowing ongoing workloads on these instances to complete so that a higher marginal gain may be achieved in subsequent decisions.

**Synchronization strategy.** We selectively synchronize model parameters to rollout instances only when synchronization is expected to improve system throughput (Algorithm 1, line 3). (1) First, an instance  $i$  is considered eligible for synchronization only if its local model version lags behind the PS, i.e.,  $ps\_version > S[i].inst\_version$ , and no trajectory in the TS can be routed to this instance given the staleness constraint. In this case, the instance cannot accept additional load without synchronization. (2) Second, we tentatively update the instance and execute the *routing strategy* once. If this tentative update enables new trajectories to be routed (indicating that the marginal gain exceeds the predefined threshold), we perform the synchronization to improve throughput.

**Migration strategy.** During rollout, load imbalance motivates trajectory migration across instances (Algorithm 1, line 9). We trigger migration in two cases. (1) When the KV Cache is full, `run_trajs` are preempted into `wait_trajs` (Figure 11), which do not contribute to throughput. We therefore set a threshold  $\varphi_{wait}$ : once the number of `wait_trajs` on an instance exceeds this limit, the excess trajectories are interrupted and returned to the TS for possible re-routing by the *routing strategy*. (2) When the throughput gap between the highest- and lowest-throughput instances exceeds  $\varphi_{throughput}$ , all trajectories on the highest-throughput instance are interrupted and returned to the TS for redistribution by the *routing strategy*.

## 6 Evaluations

In this section, we evaluate STALEFLOW by comparing it against a broad set of baselines to assess end-to-end system performance (§6.2) and RL convergence (§6.3). We further examine its scalability (§6.4) and provide a detailed analysis of its performance gains (§6.5).

### 6.1 Experimental Setup

**Testbed and workloads.** Our experiments use a testbed of 16 machines, each with 8 NVIDIA H20 GPUs. We adopt the DAPO algorithm [82] and train on the DAPO-Math-17k dataset [9] (consistent with prior work [41, 62]), with prompt and response length limits set to 2k and 20k, respectively. The batch size is set to 128, and the group size is set to 16, meaning each training step processes a total of 2048 trajectories. For evaluation, we use the AIME24 dataset [8].

**Models and metrics.** As summarized in Table 2, we evaluate four models from the Qwen family [55, 78], covering a range of model scales and architectures. This includes both distilled [79] and base variants, as well as both dense and mixture-of-experts (MoE) [3, 29,

**Table 2: Models and GPU allocations used in our evaluations.**

DeepSeek-R1-Distill, Dense	Base, Dense	Base, MoE
Qwen2.5-14B	Qwen2.5-32B	Qwen2.5-32B
64 GPUs	128 GPUs	128 GPUs

45] models. For each model, we allocate an appropriate cluster size to accommodate its computational requirements.

We measure system performance by reporting throughput (tokens/s), calculated as the total number of tokens processed across multiple post-training steps divided by the total execution time. To assess learning convergence, we plot reward curves during training and report the pass@1 accuracy (i.e., the proportion of problems solved correctly on the first attempt) on the evaluation set.

**Baselines and settings.** We select five baselines from three categories: (1) *No staleness*. We first compare with VeRL [63], a widely used synchronous RL system where rollout and training share the same resources and execute sequentially, without introducing data staleness. (2) *One-Step staleness*. Next, we compare with VeRL-Pipeline [18, 42], which allows only one-step asynchrony. It adopts a disaggregated architecture and overlaps rollout which is one version behind with the current training step. (3) *Strict staleness control*. These baselines share the same property as STALEFLOW, allowing a user-defined *staleness bound*  $\eta$  to tune system performance. Specifically, we compare against VeRL-Async [17], AReAL [10], and Roll Flash [41]. Although their engineering implementations differ, they all regulate staleness by limiting the amount of in-flight data and only support partial rollout (Figure 2).

In all experiments, we tune the GPU allocation ratio between rollout and training to optimal values and adopt the most efficient parallelism strategy. For STALEFLOW, the hyperparameters related to rollout coordination strategies are set as follows:  $\mu = 0.3$ ,  $\varphi_{wait} = 3$ , and  $\varphi_{throughput} = 5$ . To ensure a fair comparison, redundant rollout is not used, as it would abort trajectories and negatively affect response length. Interested readers can refer to Appendix C for additional details and an ablation study on redundant rollout.

### 6.2 End-to-End Throughput

As shown in Figure 13, we first compare the end-to-end throughput across different systems. Under varying models and *staleness bounds*, STALEFLOW consistently achieves the highest throughput. (1) Compared to synchronized systems without staleness (VeRL), STALEFLOW improves throughput by up to  $2.68 \times$  ( $2.01 \times$  on average). (2) Compared to one-step staleness systems (VeRL-Pipeline), STALEFLOW achieves up to  $1.95 \times$  ( $1.52 \times$  on average) greater improvement. (3) Compared to the best-performing system among those with strict staleness control (VeRL-Async), STALEFLOW still delivers a throughput gain of up to  $1.42 \times$  ( $1.17 \times$  on average). Furthermore, this gain increases as the *staleness bound* becomes larger.

These results can be explained as follows. (1) Synchronized systems cannot execute asynchronously and leverage stale data to mitigate skewness, resulting in the lowest throughput. (2) One-Step staleness systems cannot further improve performance by relaxing the *staleness bound*. (3) Other systems with strict staleness control (e.g., VeRL-Async, Roll Flash, AReAL) rely on simple mechanisms

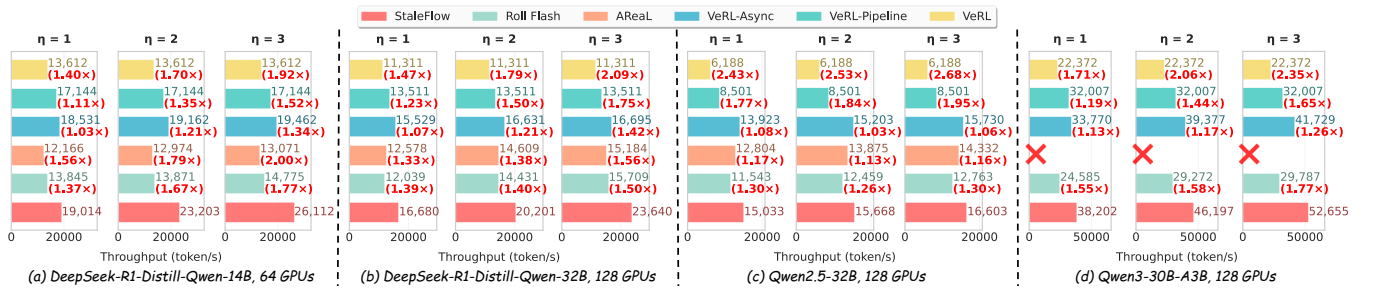


Figure 13: End-to-end throughput under different staleness bounds ( $\eta$ ). Values in parentheses are the gains achieved by STALEFLOW compared to the baselines. Red crosses denote unsupported configurations: data skewness causes severe load imbalance, leading to NCCL [20, 49] timeouts.

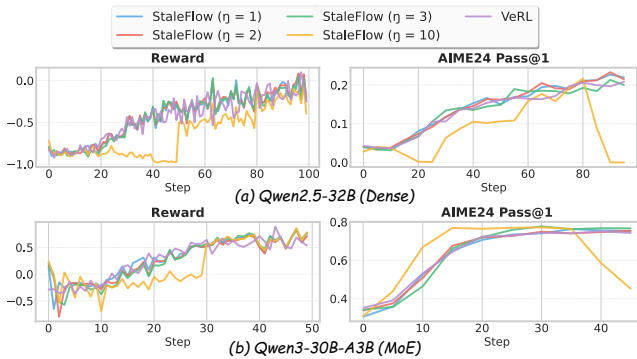


Figure 14: RL convergence comparing STALEFLOW with VeRL.

that limit the number of in-flight trajectories, preventing the use of more flexible rollout coordination techniques (Figure 2). In contrast, STALEFLOW supports a suite of staleness-aware rollout coordination strategies (§5.3) that more effectively mitigate data skewness (further evaluated in §6.5). As a result, under the same *staleness bound*, STALEFLOW can extract substantially higher throughput gains.

### 6.3 Convergence

We report reward and evaluation curves for training two base models from scratch. As shown in Figure 14, we train Qwen2.5-32B for 100 steps and Qwen3-30B-A3B for 50 steps. (1) First, when the *staleness bound* is excessively large (e.g.,  $\eta = 10$ ), training collapses entirely. This observation underscores the necessity of strict staleness control: leaving staleness unconstrained may severely degrade RL convergence. (2) Second, when the *staleness bound* is set between 1 and 3, STALEFLOW achieves convergence comparable to VeRL, the baseline with no staleness, for both dense and MoE models. These results indicate that while improving throughput, STALEFLOW can largely preserve convergence under bounded staleness.

### 6.4 Scalability

Next, we evaluate the scalability of STALEFLOW compared to representative systems of different types. Among systems with strict staleness control, VeRL-Async delivers the best performance and is therefore selected. We use the Qwen3-30B-A3B model with a

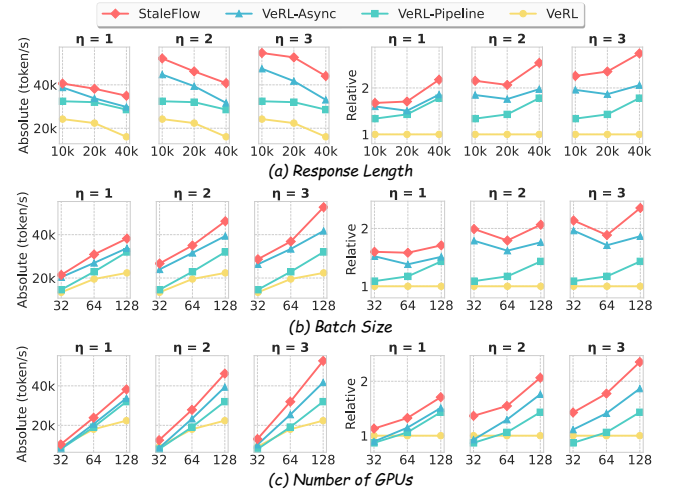


Figure 15: Absolute and relative throughput (normalized to VeRL) under different scaling factors.

response length limit of 20K, batch size of 128, and 128 GPUs, consistent with the configuration in Figure 13(d). As shown in Figure 15, we vary one factor at a time while holding the others constant.

**Response length.** Longer response lengths exacerbate long-tail effects and increase data skewness, which generally reduces system throughput. Despite this, STALEFLOW maintains the highest absolute throughput across all settings. More importantly, its throughput relative to VeRL scales better than that of other systems, underscoring its stronger ability to mitigate long-tail data skewness.

**Batch size.** Increasing batch sizes improves GPU utilization and thereby boosts throughput. Compared to baselines, STALEFLOW demonstrates superior scalability in both absolute throughput and relative gains. This indicates that STALEFLOW translates larger batches into throughput improvement more efficiently, making better use of available trajectories per post-training step.

**Number of GPUs.** Scaling the number of GPUs provides greater compute capacity, leading to higher throughput. STALEFLOW scales at least comparably to other systems, and its advantage becomes more pronounced under larger *staleness bounds*.

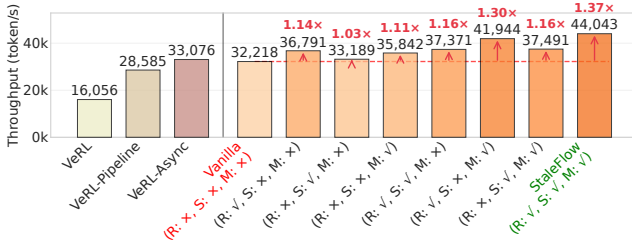


**Figure 16: Ablation study of rollout coordination strategies.** “R”, “S”, and “M” denote *routing*, *synchronization*, and *migration* strategies, respectively. “✓” indicates STALEFLOW’s throughput-oriented strategy; “×” indicates the vanilla counterpart.

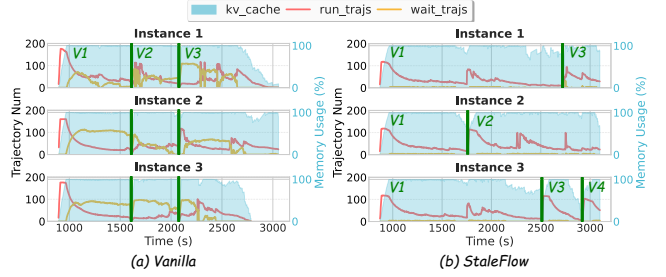
## 6.5 Performance Interpretation

We further conduct a detailed analysis to identify the sources of throughput gain and provide a detailed breakdown of STALEFLOW. The analysis uses a representative configuration: Qwen3-30B-A3B on 128 GPUs, with a batch size of 128, group size of 16, response length of 40K, and a *staleness bound* of 3.

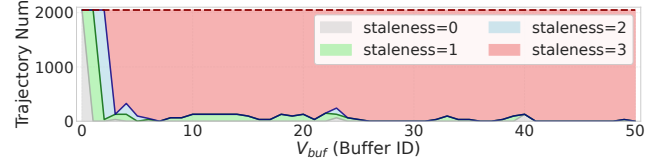
**Ablation study.** Corresponding to the three throughput-oriented rollout coordination strategies in STALEFLOW, we implement three vanilla counterparts for comparison: (1) *Vanilla routing*. Trajectories are assigned purely by load balancing their counts. Each trajectory in TS is routed to the instance with the fewest trajectories. (2) *Vanilla synchronization*. Model updates are performed greedily. An instance synchronizes the model immediately once a newer version is observed at the PS. (3) *Vanilla migration*. No proactive migration is applied. Trajectories migrate only passively upon synchronization interruptions, after being returned to the TS and re-routed.

Figure 16 shows the results under different combinations of throughput-oriented and vanilla strategies. First, when all vanilla strategies are used, performance closely matches that of VeRL-Async, confirming that the gains of STALEFLOW do not stem from engineering artifacts. Second, progressively replacing vanilla strategies with those of STALEFLOW consistently improves throughput, with the highest gain achieved when all three strategies are enabled. We interpret these results as follows. (1) *Vanilla routing* balances trajectory counts but fails to balance or optimize per-instance throughput. (2) *Vanilla synchronization* triggers more frequent model updates, which interrupt more ongoing trajectories and incur extra KV Cache recomputation overhead. In contrast, STALEFLOW synchronizes per instance based on actual load, significantly reducing this overhead. (3) *Vanilla migration* lacks proactive redistribution, making it hard to rebalance the workload once skewness occurs.

**Case study.** To better illustrate the effect of each strategy, we present the per-instance rollout load over 3000 seconds when using all STALEFLOW strategies versus all vanilla counterparts. As shown in Figure 17, we observe: (1) *Vanilla routing* distributes all assignable trajectories evenly across instances, while STALEFLOW routes based on the marginal throughput gain threshold  $\mu$ . For example, in Figure 17(b), each instance initially receives only about 100 trajectories, with the rest kept at the TS. This leaves more flexibility for subsequent adjustments when load imbalance emerges. (2) *Vanilla*



**Figure 17: Per-Instance rollout load over time.** The green lines indicate model synchronizations and tags indicate model versions.



**Figure 18: Trajectory staleness distribution across different staleness buffers.** The *staleness bound*  $\eta$  is set to 3.

*synchronization* performs greedy global updates even while many trajectories are still running. In Figure 17(a), instance 2 updates from  $V_2$  to  $V_3$  during heavy execution, incurring extra KV Cache recomputation overhead. STALEFLOW, however, synchronizes per instance, following each instance’s own pace. (3) *Vanilla migration* does not proactively redistribute trajectories, leading to growing waiting queues and load imbalance, whereas STALEFLOW continuously migrates trajectories via the TS, preventing this imbalance.

**Staleness distribution.** We next investigate the staleness distribution of different trajectories in each staleness buffer (i.e.,  $V_{buf} - V_{traj}$ ). As shown in Figure 18, we observe that: (1) No trajectory exceeds a staleness of 3, meaning all trajectories satisfy the constraint  $V_{traj} + 3 \geq V_{buf}$ . This reflects the effectiveness of our global consistency protocol in achieving strict staleness control while supporting flexible rollout coordination. (2) As training proceeds, most buffers contain only trajectories with staleness 3. This indicates that STALEFLOW fully exploits the maximum bound  $\eta$  to squeeze out system throughput by tolerating higher staleness where possible.

**Time breakdown.** As presented in Table 3, we report the average per-step rollout time, which also constitutes the total RL post-training step time (since the reward and training phases are overlapped by the rollout phase). It can be observed that per-token decoding during trajectory generation accounts for the majority of the time (89.9%). Meanwhile, KV Cache prefill or re-prefill after trajectory routing or migration takes 7.9%. The overhead induced by STALEFLOW’s rollout commands remains below 3%. Specifically, the Route and Interrupt commands for trajectories only involve communicating lightweight tokens, thus consuming merely 0.5%, whereas Pull requires transferring larger model parameters and hence takes longer, but still only 1.7%. Furthermore, we compare the model synchronization time under different configurations with

**Table 3: Rollout execution time breakdown (per-step).**

STALEFLOW’s Rollout Commands			Trajectory Generation	
Pull	Route	Interrupt	Prefill	Decode
7.8s (1.7%)	2.0s (0.4%)	0.6s (0.1%)	36.4s (7.9%)	413.3s (89.9%)

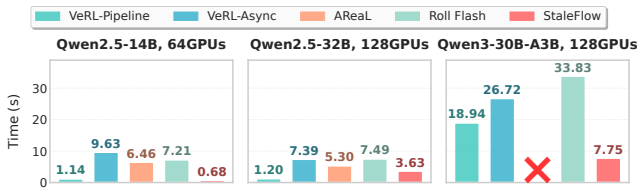


**Figure 19: Overhead of model synchronization.**

other baselines, as shown in Figure 19. STALEFLOW achieves the minimal latency in most settings. This demonstrates that the additionally introduced TS and PS, along with the various rollout commands designed atop them, introduce negligible overhead.<sup>3</sup>

## 7 Related Work

**RL post-training systems.** A number of RL post-training systems have emerged recently. Early systems largely adopted synchronous architectures with shared resources [19, 28, 43, 63, 70, 77, 95], while more recent efforts have shifted toward asynchronous and disaggregated designs [10, 15, 16, 41, 42, 48, 62, 76, 94]. These works propose various rollout coordination techniques to mitigate data skewness (see §2.3). However, most of them are ad hoc, and none of the existing systems provides a comprehensive staleness control protocol. As a result, they cannot perform holistic global optimization to mitigate data staleness under a bounded staleness.

In addition, several works focus on improving the efficiency of rollout itself, for example, by reducing generation latency via speculative decoding [4, 16, 37, 54, 60] or low-precision quantization [21, 41]. These efficient RL optimizations are orthogonal to our work and can be seamlessly incorporated into STALEFLOW.

**Optimizing training and generation.** Significant progress has been made in training through hybrid parallelisms, including data parallelism [56, 88], tensor parallelism [47, 64], pipeline parallelism [22, 24, 46], sequence parallelism [23, 38], and expert parallelism [29]. Systems such as Megatron [47, 64] and DeepSpeed [23, 56] have integrated multiple parallelisms, while many works [31, 32, 44, 71] further enable automatic parallelization tuning. For model generation, numerous optimizations have been proposed, including speculative decoding [30], chunked prefill [1], prefill-decode disaggregation [93], prefix caching [34], KV Cache quantization [84], and other management strategies [11]. Many of these techniques have been integrated into systems such as vLLM [27] and SGLang [92].

<sup>3</sup>In addition, the overhead of Algorithm 1 is typically under 0.1s, which continuously runs in the background process of the rollout coordinator.

All these training and generation optimizations are applicable to STALEFLOW. By adopting a fully disaggregated architecture, STALEFLOW cleanly decouples rollout (generation) and training, allowing each RL phase to be optimized independently.

**Optimizing data skewness.** Data skewness caused by variable-length sequences is a well-known problem for large models. Existing systems have tackled it during model pre-training [13, 33, 72], fine-tuning [2, 36], and serving [75], typically by dynamically adapting parallelism strategies to accommodate varying lengths. In contrast, STALEFLOW targets data skewness specifically in RL post-training. Compared to other scenarios, RL introduces an additional challenge: data staleness, which does not arise in conventional training or serving pipelines. It is tightly coupled with data skewness and must be optimized jointly. This makes our target setting fundamentally more complex, as STALEFLOW must prioritize convergence while maximizing system performance. Consequently, STALEFLOW incorporates staleness constraints into its data management design.

## 8 Conclusion and Future Work

This work presents STALEFLOW, a fully disaggregated RL post-training system that jointly addresses data staleness and data skewness. STALEFLOW introduces a global consistency protocol that enables fine-grained staleness control, together with architectural and algorithmic innovations that support staleness-aware, throughput-oriented rollout coordination strategies for mitigating skewness. While preserving RL convergence, STALEFLOW achieves up to 1.42-2.68× (1.17-2.01× on average) higher throughput than state-of-the-art RL post-training systems. As future work, we plan to extend STALEFLOW to support a broader range of RL tasks (e.g., coding, agent-based, and multi-turn responses) and a wider spectrum of models (e.g., multi-modal). Since STALEFLOW is agnostic to the types of tasks and models, it is broadly applicable.

## References

- [1] Amey Agrawal, Nitin Kedia, Ashish Panwar, Jayashree Mohan, Nipun Kwatra, Bhargav Gulavani, Alexey Tumanov, and Ramachandran Ramjee. Taming Throughput-Latency tradeoff in LLM inference with Sarathi-Serve. In *18th USENIX Symposium on Operating Systems Design and Implementation (OSDI 24)*, 2024. <https://www.usenix.org/conference/osdi24/presentation/agrawal>.
- [2] Yushi Bai, Xin Lv, Jiajie Zhang, Yuze He, Ji Qi, Lei Hou, Jie Tang, Yuxiao Dong, and Juanzi Li. Longalign: A recipe for long context alignment of large language models, 2024. <https://arxiv.org/abs/2401.18058>.
- [3] Weilin Cai, Juyong Jiang, Fan Wang, Jing Tang, Sunghun Kim, and Jiayi Huang. A survey on mixture of experts in large language models. *IEEE Transactions on Knowledge and Data Engineering*, 2025. <http://dx.doi.org/10.1109/TKDE.2025.3554028>.
- [4] Qiaoling Chen, Zijun Liu, Peng Sun, Shenggui Li, Guoteng Wang, Ziming Liu, Yonggang Wen, Siyuan Feng, and Tianwei Zhang. Respec: Towards optimizing speculative decoding in reinforcement learning systems, 2025. <https://arxiv.org/abs/2510.26475>.
- [5] DeepSeek-AI, Daya Guo, Dejian Yang, et al. Deepseek-r1: Incentivizing reasoning capability in llms via reinforcement learning, 2025. <https://arxiv.org/abs/2501.12948>.
- [6] Dong Du, Shulin Liu, Tao Yang, Shaohua Chen, and Yang Li. Ulorl: an ultra-long output reinforcement learning approach for advancing large language models’ reasoning abilities, 2025. <https://arxiv.org/abs/2507.19766>.
- [7] Victor Elvira and Luca Martino. Advances in importance sampling. *Wiley StatsRef: Statistics Reference Online*, 2021. <http://dx.doi.org/10.1002/9781118445112.stats08284>.
- [8] Hugging Face. Aime24 dataset, 2025. <https://huggingface.co/datasets/math-ai/aime24>.
- [9] Hugging Face. Dapo-math-17k dataset, 2025. <https://huggingface.co/datasets/BitedTsinghua-SIA/DAPO-Math-17k>.

[10] Wei Fu, Jiaxuan Gao, Xujie Shen, Chen Zhu, Zhiyu Mei, Chuyi He, Shusheng Xu, Guo Wei, Jun Mei, Jiahu Wang, Tongkai Yang, Binhang Yuan, and Yu Wu. Areal: A large-scale asynchronous reinforcement learning system for language reasoning, 2025. <https://arxiv.org/abs/2505.24298>.

[11] Shihong Gao, Xin Zhang, Yanyan Shen, and Lei Chen. Apt-serve: Adaptive request scheduling on hybrid cache for scalable llm inference serving. *Proc. ACM Manag. Data*, 2025. <https://doi.org/10.1145/3725394>.

[12] Wei Gao, Yuheng Zhao, Dakai An, Tianyuan Wu, Lunxi Cao, Shaopan Xiong, Ju Huang, Weixun Wang, Siran Yang, Wenbo Su, Jiamang Wang, Lin Qu, Bo Zheng, and Wei Wang. Rollpacker: Mitigating long-tail rollouts for fast, synchronous rl post-training, 2025. <https://arxiv.org/abs/2509.21009>.

[13] Hao Ge, Fangcheng Fu, Haoyang Li, Xuanyu Wang, Sheng Lin, Yujie Wang, Xiaonan Nie, Hailin Zhang, Xupeng Miao, and Bin Cui. Enabling parallelism hot switching for efficient training of large language models. In *Proceedings of the ACM SIGOPS 30th Symposium on Operating Systems Principles*, 2024. <https://doi.org/10.1145/3694175.3695969>.

[14] Dan Halbersberg, Matan Halevi, and Moshe Salhov. Search and score-based waterfall auction optimization. In *Learning and Intelligent Optimization: 16th International Conference, LION 16, Milos Island, Greece, June 5–10, 2022, Revised Selected Papers*, 2022. [https://doi.org/10.1007/978-3-031-24866-5\\_27](https://doi.org/10.1007/978-3-031-24866-5_27).

[15] Zhenyu Han, Ansheng You, Haibo Wang, Kui Luo, Guang Yang, Wenqi Shi, Menglong Chen, Sicheng Zhang, Zeshun Lan, Chunshi Deng, Huazhong Ji, Wenjie Liu, Yu Huang, Yixiang Zhang, Chenyi Pan, Jing Wang, Xin Huang, Chunsheng Li, and Jianping Wu. Asyncflow: An asynchronous streaming rl framework for efficient llm post-training, 2025. <https://arxiv.org/abs/2507.01663>.

[16] Jingkai He, Tianjian Li, Erhu Feng, Dong Du, Qian Liu, Tao Liu, Yubin Xia, and Haibo Chen. History rhymes: Accelerating llm reinforcement learning with rhymrl, 2025. <https://arxiv.org/abs/2508.18588>.

[17] <https://github.com/meituan/search>. Verl recipe: Fully async policy trainer, 2025. [https://verl.readthedocs.io/en/latest/advance/fully\\_async.html](https://verl.readthedocs.io/en/latest/advance/fully_async.html).

[18] <https://github.com/meituan/search>. Verl recipe: One step off policy async trainer, 2025. [https://verl.readthedocs.io/en/latest/advance/one\\_step\\_off.html](https://verl.readthedocs.io/en/latest/advance/one_step_off.html).

[19] Jian Hu, Xibin Wu, Wei Shen, Jason Klein Liu, Zilin Zhu, Weixun Wang, Songlin Jiang, Haoran Wang, Hao Chen, Bin Chen, Weikai Fang, Xianyu, Yu Cao, Haotian Xu, and Yiming Liu. Openrlhf: An easy-to-use, scalable and high-performance rlhf framework, 2025. <https://arxiv.org/abs/2405.11143>.

[20] Zhiyi Hu, Siyuan Shen, Tommaso Bonato, Sylvain Jeaugey, Cedell Alexander, Eric Spada, James Dinan, Jeff Hammond, and Torsten Hoefer. Demystifying nccl: An in-depth analysis of gpu communication protocols and algorithms, 2025. <https://arxiv.org/abs/2507.04786>.

[21] Wei Hu, Yi Ge, Shuai Yang, Yicheng Xiao, Huizi Mao, Yujun Lin, Hanrong Ye, Sifei Liu, Ka Chun Cheung, Hongxu Yin, Yao Lu, Xiaojuan Qi, Song Han, and Yukang Chen. Qerl: Beyond efficiency – quantization-enhanced reinforcement learning for llms, 2025. <https://arxiv.org/abs/2510.11696>.

[22] Yanping Huang, Youlong Cheng, Ankur Bapna, Orhan Firat, Mia Xu Chen, Zhipeng Chen, Yanping Hu, Maxim Krikun, Quoc V. Le, and Yonghui Chen. Gipe: Efficient training of giant neural networks using pipeline parallelism. In *Advances in Neural Information Processing Systems (NeurIPS)*, 2019. <https://proceedings.neurips.cc/paper/2019/file/093f65e080a295f8076b1c5722a46aa2-Paper.pdf>.

[23] Sam Ade Jacobs, Masahiro Tanaka, Chengming Zhang, Minjia Zhang, Reza Yazdani Aminadabi, Shuaiwen Leon Song, Samyam Rajbhandari, and Yuxiong He. System optimizations for enabling training of extreme long sequence transformer models. In *Proceedings of the 43rd ACM Symposium on Principles of Distributed Computing*, 2024. <https://doi.org/10.1145/3662158.3662806>.

[24] Chenyu Jiang, Zhen Jia, Shuai Zheng, Yida Wang, and Chuan Wu. Dynapipe: Optimizing multi-task training through dynamic pipelines. In *Proceedings of the Nineteenth European Conference on Computer Systems (EuroSys)*, 2024. <https://doi.org/10.1145/3627703.3629585>.

[25] Devvrit Khatri, Lovish Madaan, Rishabh Tiwari, Rachit Bansal, Sai Surya Duvvuri, Manzil Zaheer, Inderjit S. Dhillon, David Brandfonbrener, and Rishabh Agarwal. The art of scaling reinforcement learning compute for llms, 2025. <https://arxiv.org/abs/2510.13786>.

[26] Branislav Kveton, Saied Mahdian, S. Muthukrishnan, Zheng Wen, and Yikun Xian. Waterfall bandits: Learning to sell ads online, 2019. <https://arxiv.org/abs/1904.09404>.

[27] Woosuk Kwon, Zhuohan Li, Siyuan Zhuang, Ying Sheng, Lianmin Zheng, Cody Hao Yu, Joseph Gonzalez, Hao Zhang, and Ion Stoica. Efficient memory management for large language model serving with paginatedattention. In *Proceedings of the 29th Symposium on Operating Systems Principles*, 2023. <https://doi.org/10.1145/3600006.3613165>.

[28] Kinman Lei, Yuyang Jin, Mingshu Zhai, Kezhao Huang, Haoxing Ye, and Jidong Zhai. Puzzle: efficiently aligning large language models through light-weight context switch. In *Proceedings of the 2024 USENIX Conference on Usenix Annual Technical Conference*, 2024.

[29] Dmitry Lepikhin, HyoukJoong Lee, Yuanzhong Xu, Dehao Chen, Orhan Firat, Yanping Huang, Maxim Krikun, Noam Shazeer, and Zhipeng Chen. {GS}hard: Scaling giant models with conditional computation and automatic sharding. In *International Conference on Learning Representations*, 2021. <https://openreview.net/forum?id=qewe7XHTmYb>.

[30] Yaniv Leviathan, Matan Kalman, and Yossi Matias. Fast inference from transformers via speculative decoding. In *Proceedings of the 40th International Conference on Machine Learning*, 2023. <https://dl.acm.org/doi/10.5555/3618408.3619203>.

[31] Haoyang Li, Fangcheng Fu, Hao Ge, Sheng Lin, Xuanyu Wang, Jiawen Niu, Xupeng Miao, and Bin Cui. Hetu v2: A general and scalable deep learning system with hierarchical and heterogeneous singl program multiple data annotations, 2025. <https://arxiv.org/abs/2504.20490>.

[32] Haoyang Li, Fangcheng Fu, Hao Ge, Sheng Lin, Xuanyu Wang, Jiawen Niu, Yujie Wang, Hailin Zhang, Xiaonan Nie, and Bin Cui. Malleus: Straggler-resilient hybrid parallel training of large-scale models via malleable data and model parallelization. *Proc. ACM Manag. Data*, 2025. <https://doi.org/10.1145/3725322>.

[33] Haoyang Li, Fangcheng Fu, Sheng Lin, Hao Ge, Xuanyu Wang, Jiawen Niu, Jinbao Xue, Yangyu Tao, Di Wang, Jie Jiang, and Bin Cui. Hydraulis: Balancing large transformer model training via co-designing parallel strategies and data assignment. *Proc. ACM Manag. Data*, 2025. <https://doi.org/10.1145/3769802>.

[34] Yuhang Li, Rong Gu, Chengying Huan, Zhibin Wang, Renjie Yao, Chen Tian, and Guihai Chen. Hotprefix: Hotness-aware kv cache scheduling for efficient prefix sharing in llm inference systems. *Proc. ACM Manag. Data*. <https://doi.org/10.1145/3749168>.

[35] Hunter Lightman, Vineet Kosaraju, Yuri Burda, Harrison Edwards, Bowen Baker, Teddy Lee, Jan Leike, John Schulman, Ilya Sutskever, and Karl Cobbe. Let's verify step by step. In *The Twelfth International Conference on Learning Representations*, 2024. <https://openreview.net/forum?id=v8L0pN6Oi>.

[36] Sheng Lin, Fangcheng Fu, Haoyang Li, Hao Ge, Xuanyu Wang, Jiawen Niu, Yaofeng Tu, and Bin Cui. Lobra: Multi-tenant fine-tuning over heterogeneous data. *Proc. VLDB Endow.*, 2025. <https://doi.org/10.14778/3742728.3742752>.

[37] Bingshuai Liu, Ante Wang, Zijun Min, Liang Yao, Haibo Zhang, Yang Liu, Xu Han, Peng Li, Anxiang Zeng, and Jinsong Su. Spec-rl: Accelerating on-policy reinforcement learning with speculative rollouts, 2026. <https://arxiv.org/abs/2509.23232>.

[38] Hao Liu, Matei Zaharia, and Pieter Abbeel. Ringattent with blockwise transformers for near-infinite context. In *The Twelfth International Conference on Learning Representations*, 2024. <https://openreview.net/forum?id=WsRHpHH4s0>.

[39] Jiaci Liu, Yingru Li, Yuqian Fu, Jiawei Wang, Qian Liu, and Yu Shen. When speed kills stability: Demystifying rl collapse from the inference-training mismatch, 2025. <https://yingru.notion.site/When-Speed-Kills-Stability-Demystifying-RL-Collapse-from-the-Inference-Training-Mismatch-271211a558b7808d8b12d403fd15edda>.

[40] Liyuan Liu, Feng Yao, Dinghuai Zhang, Chengyu Dong, Jingbo Shang, and Jianfeng Gao. Flashrl: 8bit rollouts, full power rl, 2025. <https://fengyao.notion.site/flash-rl>.

[41] Han Lu, Zichen Liu, Shaopan Xiong, Yancheng He, Wei Gao, Yanan Wu, Weixun Wang, Jiashun Liu, Yang Li, Haizhou Zhao, Ju Huang, Siran Yang, Xiaoyang Li, Yijia Luo, Zihe Liu, Ling Pan, Junchi Yan, Wei Wang, Wenbo Su, Jiamang Wang, Lin Qu, and Bo Zheng. Part ii: Roll flash – accelerating rlrv and agetic training with asynchrony, 2025. <https://arxiv.org/abs/2510.11345>.

[42] Michael Luo, Sijun Tan, Roy Huang, Ameen Patel, Alpay Ariyak, Qingyang Wu, Xiaoxiang Shi, Rachel Xin, Colin Cai, Maurice Weber, Ce Zhang, Li Erran Li, Raluca Ada Popa, and Ion Stoica. Deepcoder: A fully open-source 14b coder at o3-mini level, 2025. <https://pretty-radio-b75.notion.site/DeepCoder-A-Fully-Open-Source-14B-Coder-at-O3-mini-Level-1cf81902c14680b3bee5eb349a512a51>.

[43] Zhiyi Mei, Wei Fu, Kaiwei Li, Guangyu Wang, Huanchen Zhang, and Yi Wu. Real: Efficient rlhf training of large language models with parameter reallocation. In *Eighth Conference on Machine Learning and Systems*, 2025. <https://openreview.net/forum?id=yLU1zRf95d>.

[44] Xupeng Miao, Yujie Wang, Youhe Jiang, Chunan Shi, Xiaonan Nie, Hailin Zhang, and Bin Cui. Galvatron: Efficient transformer training over multiple gpus using automatic parallelism. *Proc. VLDB Endow.*, 2022. <https://doi.org/10.14778/3570690.3570697>.

[45] Siyuan Mu and Sen Lin. A comprehensive survey of mixture-of-experts: Algorithms, theory, and applications, 2025. <https://arxiv.org/abs/2503.07137>.

[46] Deepak Narayanan, Aaron Harlap, Amar Phanishayee, Vivek Seshadri, Nikhil R. Devanur, Gregory R. Ganger, Phillip B. Gibbons, and Matei Zaharia. Pipedream: generalized pipeline parallelism for dnn training. In *Proceedings of the 27th ACM Symposium on Operating Systems Principles*, 2019. <https://doi.org/10.1145/3341301.3359646>.

[47] Deepak Narayanan, Mohammad Shoeybi, Jared Casper, Patrick LeGresley, Mostofa Patwary, Vijay Korthikanti, Dmitri Vainbrand, Preethvi Kashinkunti, Julie Bernauer, Bryan Catanzaro, Amar Phanishayee, and Matei Zaharia. Efficient large-scale language model training on gpu clusters using megatron-lm. In *Proceedings of the International Conference for High Performance Computing, Networking, Storage and Analysis*, 2021. <https://doi.org/10.1145/3458817.3476209>.

[48] Michael Noukhovitch, Shengyi Huang, Sophie Xhonneux, Arian Hosseini, Rishabh Agarwal, and Aaron Courville. Asynchronous rlhf: Faster and more efficient off-policy rl for language models, 2025. <https://arxiv.org/abs/2410.18252>.

[49] NVIDIA. Nvidia collective communication library (nccl) documentation, 2025. <https://docs.nvidia.com/deeplearning/nccl/user-guide/docs/index.html>.

[50] NVIDIA. Nvidia inference xfer library (nixl), 2025. <https://github.com/ai-dynamo/nixl>.

[51] OpenAI, ;, Aaron Jaech, Adam Kalai, Adam Lerer, et al. Openai o1 system card, 2024. <https://arxiv.org/abs/2412.16720>.

[52] openux. Unified communication x, 2025. <https://github.com/openux/uxc>.

[53] Aske Plaat, Annie Wong, Suzan Verberne, Joost Broekens, Niki Van Stein, and Thomas Back. Multi-step reasoning with large language models, a survey. *ACM Comput. Surv.*, 2025. <https://doi.org/10.1145/3774896>.

[54] Ruoyu Qin, Weiran He, Weixian Huang, Yangkun Zhang, Yikai Zhao, Bo Pang, Xinran Xu, Yingdi Shan, Yongwei Wu, and Mingxing Zhang. Seer: Online context learning for fast synchronous llm reinforcement learning, 2025. <https://arxiv.org/abs/2511.14617>.

[55] Qwen, ;, An Yang, Baosong Yang, Beichen Zhang, et al. Qwen2.5 technical report, 2025. <https://arxiv.org/abs/2412.15115>.

[56] Samyam Rajbhandari, Jeff Rasley, Olatunji Ruwase, and Yuxiong He. Zero: Memory optimizations toward training trillion parameter models, 2020. <https://arxiv.org/abs/1910.02054>.

[57] Z. Rosberg and I. Adiri. Multilevel queues with extremal priorities. *J. ACM*, 1976. <https://doi.org/10.1145/321978.321986>.

[58] John Schulman, Sergey Levine, Philipp Moritz, Michael Jordan, and Pieter Abbeel. Trust region policy optimization. In *Proceedings of the 32nd International Conference on International Conference on Machine Learning*, 2015. <https://dl.acm.org/doi/10.5555/3045118.3045319>.

[59] John Schulman, Filip Wolski, Prafulla Dhariwal, Alec Radford, and Oleg Klimov. Proximal policy optimization algorithms, 2017. <https://arxiv.org/abs/1707.06347>.

[60] Zelei Shao, Vikranth Srivatsa, Sanjana Srivastava, Qingyang Wu, Alpay Ariyak, Xiaoxia Wu, Ameen Patel, Jue Wang, Percy Liang, Tri Dao, Ce Zhang, Yiyi Zhang, Ben Athiwaratkun, Chenfeng Xu, and Junxiong Wang. Beat the long tail: Distribution-aware speculative decoding for rl training, 2025. <https://arxiv.org/abs/2511.13841>.

[61] Zhihong Shao, Peiyi Wang, Qihao Zhu, Runxin Xu, Junxiao Song, Xiao Bi, Haowei Zhang, Mingchuan Zhang, Y. K. Li, Y. Wu, and Daya Guo. Deepseekmath: Pushing the limits of mathematical reasoning in open language models, 2024. <https://arxiv.org/abs/2402.03300>.

[62] Guangming Sheng, Yuxuan Tong, Borui Wan, Wang Zhang, Chaobo Jia, Xibin Wu, Yuqi Wu, Xiang Li, Chi Zhang, Yanghua Peng, Haibin Lin, Xin Liu, and Chuan Wu. Laminar: A scalable asynchronous rl post-training framework, 2025. <https://arxiv.org/abs/2510.12633>.

[63] Guangming Sheng, Chi Zhang, Zilingfeng Ye, Xibin Wu, Wang Zhang, Ru Zhang, Yanghua Peng, Haibin Lin, and Chuan Wu. Hybridflow: A flexible and efficient rlhf framework. In *Proceedings of the Twentieth European Conference on Computer Systems*, 2025. <http://dx.doi.org/10.1145/3689031.3696075>.

[64] Mohammad Shoeybi, Mostofa Patwary, Raul Puri, Patrick LeGresley, Jared Casper, and Bryan Catanzaro. Megatron-lm: Training multi-billion parameter language models using model parallelism, 2020. <https://arxiv.org/abs/1909.08053>.

[65] Zelin Tan, Hejia Geng, Mulei Zhang, Xiaohang Yu, Guancheng Wan, Yifan Zhou, Qiang He, Xiangyuan Xue, Heng Zhou, Yutao Fan, Zhongzhi Li, Zaibin Zhang, Guibin Zhang, Chen Zhang, Zhenfei Yin, and Lei Bai. Scaling behaviors of llm reinforcement learning post-training: An empirical study in mathematical reasoning, 2025. <https://arxiv.org/abs/2509.25300>.

[66] Kimi Team, Yifan Bai, Yiping Bao, et al. Kimi k2: Open agentic intelligence, 2025. <https://arxiv.org/abs/2507.20534>.

[67] Kimi Team, Angang Du, Bofei Gao, et al. Kimi k1.5: Scaling reinforcement learning with llms, 2025. <https://arxiv.org/abs/2501.12599>.

[68] Surya T. Tokdar and Robert E. Kass. Importance sampling: a review. *WIREs Comput. Stat.*, 2010. <https://doi.org/10.1002/wics.56>.

[69] Peng-Yuan Wang, Tian-Shuo Liu, Chenyang Wang, Ziniu Li, Yidi Wang, Shu Yan, Chengxing Jia, Xu-Hui Liu, Xinwei Chen, Jiacheng Xu, and Yang Yu. A survey on large language models for mathematical reasoning. *ACM Comput. Surv.*, 2025. <https://doi.org/10.1145/3786333>.

[70] Weixun Wang, Shaopan Xiong, Gengru Chen, Wei Gao, et al. Reinforcement learning optimization for large-scale learning: An efficient and user-friendly scaling library, 2025. <https://arxiv.org/abs/2506.06122>.

[71] Yujie Wang, Youhe Jiang, Xupeng Miao, Fangcheng Fu, Shengan Zhu, Xiaonan Nie, Yaofeng Tu, and Bin Cui. Improving automatic parallel training via balanced memory workload optimization. *IEEE Transactions on Knowledge and Data Engineering*, August 2024. <http://dx.doi.org/10.1109/TKDE.2024.3370614>.

[72] Yujie Wang, Shiju Wang, Shengan Zhu, Fangcheng Fu, Xinyi Liu, Xuefeng Xiao, Huixia Li, Jiashi Li, Faming Wu, and Bin Cui. Flexsp: Accelerating large language model training via flexible sequence parallelism. In *Proceedings of the 30th ACM International Conference on Architectural Support for Programming Languages and Operating Systems, Volume 2*, 2025. <https://doi.org/10.1145/3676641.3715998>.

[73] Xumeng Wen, Zihan Liu, Shun Zheng, Shengyu Ye, Zhirong Wu, Yang Wang, Zhijian Xu, Xiao Liang, Junjie Li, Ziming Miao, Jiang Bian, and Mao Yang. Reinforcement learning with verifiable rewards implicitly incentivizes correct reasoning in base llms, 2025. <https://arxiv.org/abs/2506.14245>.

[74] Marvin Williams and Peter Sanders. The multiqueue: A simple and fast relaxed concurrent priority queue. *ACM Trans. Parallel Comput.*, 2025. <https://doi.org/10.1145/3771738>.

[75] Bingyang Wu, Shengyu Liu, Yinmin Zhong, Peng Sun, Xuanzhe Liu, and Xin Jin. Loongserve: Efficiently serving long-context large language models with elastic sequence parallelism. In *Proceedings of the ACM SIGOPS 30th Symposium on Operating Systems Principles*, 2024.

[76] Bo Wu, Sid Wang, Yunhao Tang, Jia Ding, Eryk Helenowski, Liang Tan, Tengyu Xu, Tushar Gowda, Zhengxing Chen, Chen Zhu, Xiaocheng Tang, Yundi Qian, Beibei Zhu, and Rui Hou. Llamarl: A distributed asynchronous reinforcement learning framework for efficient large-scale llm training, 2025. <https://arxiv.org/abs/2505.24034>.

[77] Youshua Xiao, Zhenglei Zhou, Fagui Mao, Weichang Wu, Shangchun Zhao, Lin Ju, Lei Liang, Xiaolu Zhang, and Jun Zhou. An adaptive placement and parallelism framework for accelerating rlhf training, 2024. <https://arxiv.org/abs/2312.11819>.

[78] An Yang, Anfeng Li, Baosong Yang, et al. Qwen3 technical report, 2025. <https://arxiv.org/abs/2505.09388>.

[79] Chuanyang Yang, Yao Zhu, Wang Lu, Yidong Wang, Qian Chen, Chenlong Gao, Bingjie Yan, and Yiqiang Chen. Survey on knowledge distillation for large language models: Methods, evaluation, and application. *ACM Trans. Intell. Syst. Technol.*, 2025. <https://doi.org/10.1145/3699518>.

[80] Feng Yao, Liuyan Liu, Dinghuai Zhang, Chengyu Dong, Jingbo Shang, and Jianfeng Gao. Your efficient rl framework secretly brings you off-policy rl training, 2025. <https://fengyao.notion.site/off-policy-rl>.

[81] Zihao Ye, Lequin Chen, Ruihang Lai, Wuwei Lin, Yineng Zhang, Stephanie Wang, Tianqi Chen, Baris Kasikci, Vinod Grover, Arvind Krishnamurthy, and Luis Ceze. Flashinfer: Efficient and customizable attention engine for LLM inference serving. In *Eighth Conference on Machine Learning and Systems*, 2025. <https://openreview.net/forum?id=RXPofAsL8F>.

[82] Qiying Yu, Zheng Zhang, Ruofei Zhu, Yufeng Yuan, Xiaochen Zuo, Yu Yue, Weinan Dai, Tiantian Fan, Gaohong Liu, Lingjin Liu, Xin Liu, Haibin Lin, Zhiqi Lin, Bole Ma, Guangming Sheng, Yuxuan Tong, Chi Zhang, Mofan Zhang, Wang Zhang, Hang Zhu, Jinhua Zhu, Jiaze Chen, Jianguie Chen, Chengyi Wang, Hongli Yu, Yuxuan Song, Xiangpeng Wei, Hao Zhou, Jingjing Liu, Wei-Ying Ma, Ya-Qin Zhang, Lin Yan, Mu Qiao, Yonghui Wu, and Mingxuan Wang. Dapo: An open-source llm reinforcement learning system at scale, 2025. <https://arxiv.org/abs/2503.14476>.

[83] Yang Yue, Zhiqi Chen, Rui Lu, Andrew Zhao, Zhaokai Wang, Yang Yue, Shiji Song, and Gao Huang. Does reinforcement learning really incentivize reasoning capacity in LLMs beyond the base model? In *2nd AI for Math Workshop @ ICML 2025*, 2025. <https://openreview.net/forum?id=upehLVgg1b>.

[84] Hailin Zhang, Xiaodong Ji, Yilin Chen, Fangcheng Fu, Xupeng Miao, Xiaonan Nie, Weipeng Chen, and Bin Cui. Pqcache: Product quantization-based kvcache for long context llm inference. *Proc. ACM Manag. Data*, 2025. <https://doi.org/10.1145/3725338>.

[85] Kaiyan Zhang, Yuxin Zuo, Bingxiang He, et al. A survey of reinforcement learning for large reasoning models, 2025. <https://arxiv.org/abs/2509.08827>.

[86] Yiqi Zhang, Huiqiang Jiang, Xufang Luo, Zhihe Yang, Chengruidong Zhang, Yifei Shen, Dongsheng Li, Yuqing Yang, Lili Qiu, and Yang You. SortedRL: Accelerating RL training for LLMs through online length-aware scheduling. In *ES-FoMo III: 3rd Workshop on Efficient Systems for Foundation Models*, 2025. <https://openreview.net/forum?id=YoV9lIZZ87>.

[87] Xin Zhao, Yongkang Liu, Kuan Xu, Jia Guo, Zihao Wang, Yan Sun, Xinyu Kong, Qianggang Cao, Liang Jiang, Zujie Wen, Zhiqiang Zhang, and Jun Zhou. Small leak can sink a great ship--boost rl training on moe with icepop!, 2025. <https://ringtech.notion.site/icepop>.

[88] Yanli Zhao, Andrew Gu, Rohan Varma, Liang Luo, Chien-Chin Huang, Min Xu, Less Wright, Hamid Shojanazeri, Myle Ott, Sam Shleifer, Alban Desmaison, Can Baloiglu, Pritam Damania, Bernard Nguyen, Geeta Chauhan, Yuchen Hao, Ajit Mathews, and Shen Li. Pytorch fsdp: Experiences on scaling fully sharded data parallel. *Proc. VLDB Endow.*, 2023. <https://doi.org/10.14778/3611540.3>.

[89] Chujie Zheng, Kai Dang, Bowen Yu, Mingze Li, Huiqiang Jiang, Junrong Lin, Yuqiong Liu, Hao Lin, Chencan Wu, Feng Hu, An Yang, Jingren Zhou, and Junyang Lin. Stabilizing reinforcement learning with llms: Formulation and practices, 2025. <https://arxiv.org/abs/2512.01374>.

[90] Chujie Zheng, Shixuan Liu, Mingze Li, Xiong-Hui Chen, Bowen Yu, Chang Gao, Kai Dang, Yuqiong Liu, Rui Men, An Yang, Jingren Zhou, and Junyang Lin. Group sequence policy optimization, 2025. <https://arxiv.org/abs/2507.18071>.

[91] Haizhong Zheng, Jiawei Zhao, and Beidi Chen. Prosperity before collapse: How far can off-policy rl reach with stale data on llms?, 2025. <https://arxiv.org/abs/2510.01161>.

[92] Lianmin Zheng, Liangsheng Yin, Zhiqiang Xie, Chuyue Sun, Jeff Huang, Cody Hao Yu, Shiyi Cao, Christos Kozyrakis, Ion Stoica, Joseph E. Gonzalez, Clark Barrett, and Ying Sheng. Sclang: efficient execution of structured language model programs. In *Proceedings of the 38th International Conference on Neural Information Processing Systems*, 2024. <https://dl.acm.org/doi/10.5555/3737916.3739916>.

[93] Yinmin Zhong, Shengyu Liu, Junda Chen, Jianbo Hu, Yibo Zhu, Xuanzhe Liu, Xin Jin, and Hao Zhang. Distserve: disaggregating prefill and decoding for goodput-optimized large language model serving. In *Proceedings of the 18th USENIX Conference on Operating Systems Design and Implementation*, 2024.

- [94] Yinmin Zhong, Zili Zhang, Xiaoniu Song, Hanpeng Hu, Chao Jin, Bingyang Wu, Nuo Chen, Yukun Chen, Yu Zhou, Changyi Wan, Hongyu Zhou, Yimin Jiang, Yibo Zhu, and Daxin Jiang. Streamrl: Scalable, heterogeneous, and elastic rl for llms with disaggregated stream generation, 2025. <https://arxiv.org/abs/2504.15930>.
- [95] Yinmin Zhong, Zili Zhang, Bingyang Wu, Shengyu Liu, Yukun Chen, Changyi Wan, Hanpeng Hu, Lei Xia, Runchen Ming, Yibo Zhu, and Xin Jin. Optimizing rlhf training for large language models with stage fusion. In *Proceedings of the 22nd USENIX Symposium on Networked Systems Design and Implementation*, 2025. <https://dl.acm.org/doi/10.5555/3767955.3767981>.
- [96] Yuzhen Zhou, Jiajun Li, Yusheng Su, Gowtham Ramesh, Zilin Zhu, Xiang Long, Chenyang Zhao, Jin Pan, Xiaodong Yu, Ze Wang, Kangrui Du, Jialian Wu, Ximeng Sun, Jiang Liu, Qiaolin Yu, Hao Chen, Zicheng Liu, and Emad Barsoum. April: Active partial rollouts in reinforcement learning to tame long-tail generation, 2025. <https://arxiv.org/abs/2509.18521>.

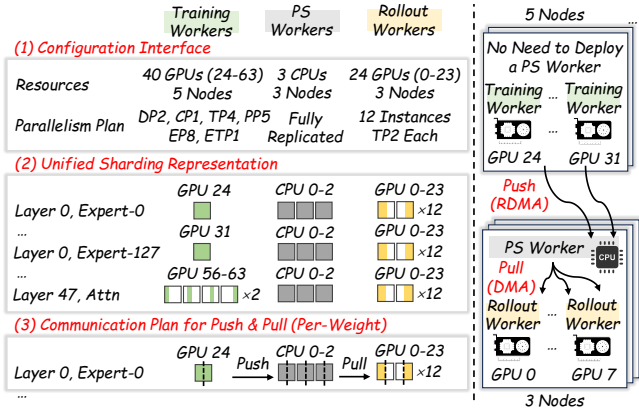


**Figure 20:** Deployment of the Qwen3-30B-A3B model across 64 H20 GPUs. (Left) The PS adopts a worker-based architecture consistent with both the training and rollout phases, supporting flexible resource placement and parallelism. The labels “DP, CP, TP, PP, EP, ETP” refer to different parallelisms—data, context, tensor, pipeline, expert, and expert-specific tensor parallelism—that collectively determine how model parameters are distributed and assigned to resources. (Right) The illustration of the deployment strategy used for Pull and Push.

## A Implementation

STALEFlow is implemented in approximately 22k lines of code (LoC) in Python. (1) The staleness manager, which enforces the global consistency protocol, accounts for around 2k LoC. (2) On the training side, STALEFlow supports the Megatron [47, 64] and FSDP2 [88] backends (Megatron is used in our evaluation) and consists of nearly 2k LoC. (3) The rollout side (i.e., the rollout service) consists of roughly 10k LoC, with approximately 3k LoC dedicated to the core logic of rollout generation using vLLM [27], 2k LoC for the rollout coordinator, 1k LoC for the trajectory server (TS), and 4k LoC for the parameter server (PS).

For efficient communication of parameters on the PS, we leverage the NVIDIA Inference Xfer Library (NIXL) [50]. NIXL builds on Unified Communication X (UCX) [52], which abstracts point-to-point (P2P) communication across various hardware (GPU/CPU/Storage), hiding the memory and communication details specific to each hardware. This abstraction enables the PS to be deployed on CPUs while ensuring efficient communication with GPUs used in both training and rollout. In the following, we provide a detailed walk-through of the PS deployment (Appendix A.1), its communication optimizations (Appendix A.2) and its scalability analysis (Appendix A.3).

### A.1 Parameter Server Deployment

The PS operates as a distributed data plane that utilizes only CPU resources, serving as middleware between the training and rollout phases. As illustrated in Figure 20 (left), the deployment follows a three-step process: (1) The PS is instantiated as a collection of workers, with resource allocation and parallelism plans specified through a unified interface, which is also used to configure training and rollout workers. This configuration defines how model

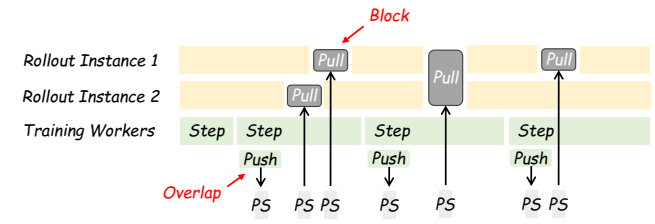


**Figure 21:** Push is triggered automatically by training workers and can overlap with the next training step, whereas Pull is issued by the rollout coordinator and must block the generation of target instances.

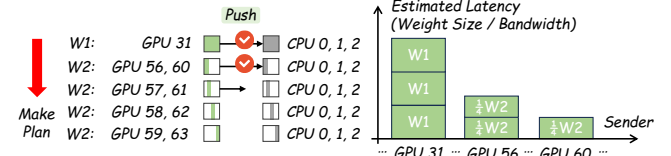


**Figure 22:** Load-balancing communication planning for Push. The estimated latency is computed by dividing the data size of the current slice (in bytes) by the bandwidth between the sender and receiver (in bytes/s), plus a constant latency term (in s). Both the bandwidth and the constant latency term can be profiled in advance.

parameters are partitioned among resources according to the parallelism plan. (2) A converter standardizes the various parallelism representations used by the training, PS, and rollout phases into STALEFlow’s unified sharding representation, ensuring consistency in parameter names and slicing granularity. (3) Synchronization is achieved through Push operations from training workers to PS workers and Pull commands from PS workers to rollout workers. Both of them are governed by load-balancing communication plans (detailed in Appendix A.2) that optimize the sending and receiving of parameter slices, minimizing overall communication latency.

As shown in Figure 21, Pull blocks the rollout generation. However, Push can overlap with the subsequent training step, since it only needs to complete before the optimizer applies the parameter updates. Consequently, the non-overlapped cost of Pull becomes a more critical performance concern. Motivated by this, as shown in Figure 20 (right), we deploy PS workers on the same nodes as rollout workers and use the fully replicated strategy, so that Pull only involves PCIe DMA copy, which is significantly faster, while Push leverages RDMA across nodes.

### A.2 Load-Balancing Communication Plan

The communication plan governs how model parameter slices are communicated across resources during Push and Pull. As shown in Figure 22, we describe the process using Push as an example.

To formulate the Push communication plan, we begin by aligning the smallest granularity of parameter slicing. With this common slicing granularity established, the next step is to determine optimal P2P pairs between senders and receivers for each parameter slice. Here, a single slice may originate from multiple potential senders but must reach one or more specific receivers. To balance

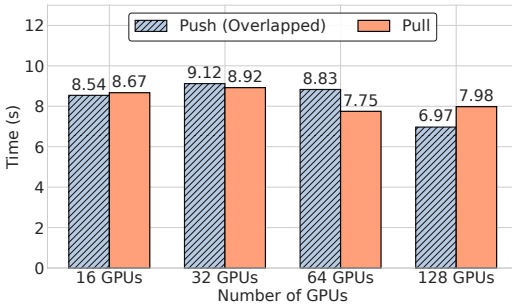


Figure 23: Communication overhead across varying cluster scales.

the communication load across senders, we track for each sender an accumulated estimate of the communication latency its assigned slices would incur. When assigning a sender for a receiver’s required slice, our planner selects the candidate sender with the smallest current accumulated latency, thereby greedily distributing traffic to minimize bottlenecks. Once obtained, this set of sender-receiver mappings is kept static and reused for every subsequent Push.

### A.3 Scalability

We evaluate the scalability of model parameter synchronization under our PS architecture. Using the Qwen3-30-A3B model, we measure the overhead of the Push (which is overlapped with training) and Pull across 16 to 128 GPUs. As shown in Figure 23, increasing the cluster size does not lead to higher communication overhead. This is because, as the cluster expands, the number of rollout workers, training workers, and PS workers increases proportionally, with additional model replicas. The optimal communication plans for small and large-scale setups exhibit similar patterns: replicas communicate independently and concurrently, balancing the load without interference. Therefore, proportionally scaling the number of model replicas does not affect communication overhead, demonstrating that the PS design exhibits good scalability.

## B Cost Model

In this section, we present the detailed derivation of our cost model  $\mathcal{T}_i(S)$ , which represents the estimated generation throughput of instance  $i$  given the snapshot  $S$  (Appendix B.1). We then compare these estimates with the actual measured throughput to assess the accuracy of our cost model (Appendix B.2).

### B.1 Derivation

Since decoding occupies most of the time during rollout (see Table 3), we simplify the throughput estimation by treating the pure decoding throughput as the overall generation throughput. It can be obtained by dividing the number of running trajectories by the per-decoding-step latency.

Following prior work [93], we model the per-decoding-step latency as the sum of the latencies of its primary computational components. The dominant components are the attention operation and the feed-forward network (FFN), which primarily consist of multiple matrix multiplications.

Table 4: Coefficients of the cost model for Qwen3-30B-A3B. These coefficients are derived via offline profiling and utilized for estimating the system’s throughput and marginal throughput gain.

Coefficients	Values
$k_1$	$7.28 \times 10^{-8}$
$k_2$	$1.72 \times 10^{-3}$
$k_3$	$1.25 \times 10^{-4}$
$k_4$	$1.07 \times 10^{-2}$

**Latency of a single operator.** In GPU execution, the latency of an operator is determined by the slower of its memory access latency and its computation latency:

$$\mathcal{L} = \max(\text{memory\_latency}, \text{computation\_latency}). \quad (5)$$

**Attention latency.** The attention operation (e.g., as implemented in FlashInfer [81]) is typically memory-bandwidth bound. Its latency is dominated by the time required to read the KV Cache from GPU memory. We model it as linearly proportional to the size of the KV Cache for the instance:

$$\mathcal{L}_{attn} = k_1 \times \text{kv\_cache}. \quad (6)$$

Here,  $k_1$  is a constant coefficient representing the inverse effective memory bandwidth for accessing the KV Cache.  $\text{kv\_cache}$  denotes the total size (e.g., in bytes) of the cached keys and values for all running trajectories being processed by the instance.

**Matrix multiplication latency.** The FFN and projection layers mainly consist of matrix multiplications. Consider a general matrix multiplication of the form  $\mathbf{Y} = \mathbf{X}\mathbf{W}$ , where  $\mathbf{X} \in \mathbb{R}^{n \times h}$  is the input ( $n$  is the number of running trajectories,  $h$  is the hidden dimension) and  $\mathbf{W} \in \mathbb{R}^{h \times h'}$  is the parameter matrix.

- **Memory latency:** The dominant memory cost for this operator is reading the parameter matrix  $\mathbf{W}$  from GPU High-Bandwidth Memory (HBM), as inputs are typically already cached. This cost is proportional to the size of  $\mathbf{W}$ :

$$\text{memory\_latency}_{matmul} = A \times (h \times h'). \quad (7)$$

$A$  is a constant related to the inverse memory bandwidth for parameter access.

- **Computation latency:** The number of floating-point operations (FLOPs) is  $2 \times n \times h \times h'$ . Therefore, the computation latency is proportional to this:

$$\text{computation\_latency}_{matmul} = B \times (2 \times n \times h \times h'). \quad (8)$$

$B$  is a constant related to the inverse computational throughput (FLOP/s) of the GPU.

Applying Eq. 5, the latency of this matrix multiplication is:

$$\mathcal{L}_{matmul} = \max(A \times (h \times h'), B \times (2 \times n \times h \times h')). \quad (9)$$

This can be simplified by defining  $k_2 = A \times (h \times h')$  and  $k_3 = B \times (2 \times n \times h \times h')$ , yielding:

$$\mathcal{L}_{matmul} = \max(k_2, k_3 \times n). \quad (10)$$

The critical point where the bottleneck shifts from memory to computation occurs when  $k_3 \times n > k_2$ , i.e.,  $n > k_2/k_3$ . The ratio  $k_2/k_3$  represents the *arithmetic intensity* threshold (in FLOPs/byte) required for the operation to become compute-bound. For example,

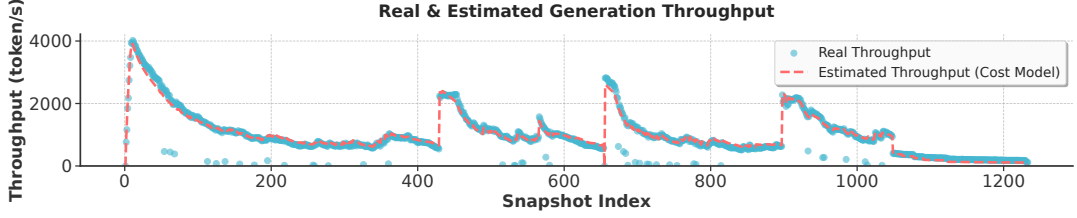


Figure 24: Comparison of actual throughput and estimated throughput from our cost model. We present the results for a single instance over the first two post-training steps.

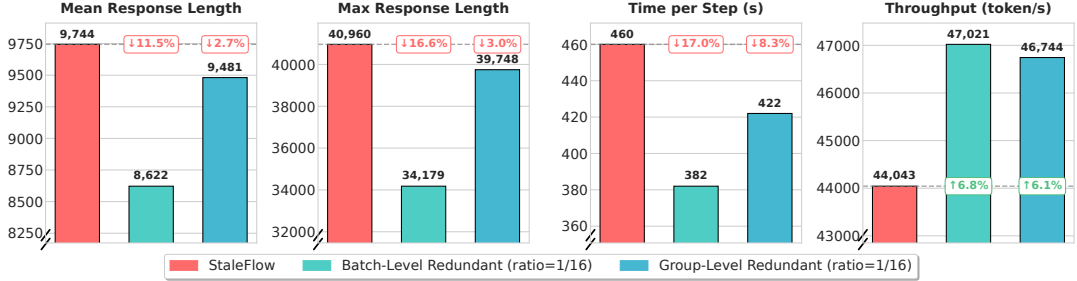


Figure 25: Effect of redundant rollout. We compare STALEFLOW with and without redundant rollout at the batch and group levels. Green bars represent performance improvements, while red bars indicate performance degradation.

with bf16 precision on an H20 GPU, this threshold is empirically found to be approximately 37. Thus, for  $n > 37$ ,  $\mathcal{L}_{matmul} \approx k_3 \times n$ .

**Total per-decoding-step latency.** Combining the latency of attention and the dominant matrix multiplication, along with a small constant overhead  $k_4$  for other operations (e.g., activation functions, layer normalization) and other latencies like kernel launch, the total per-decoding-step latency for an instance  $i$  is:

$$\begin{aligned} \mathcal{L}_i &= \mathcal{L}_{attn} + \mathcal{L}_{matmul} + k_4 \\ &= k_1 \times \text{kv\_cache}_i + \max(k_2, k_3 \times n_i) + k_4. \end{aligned} \quad (11)$$

Here,  $n_i$  represents the number of running trajectories in instance  $i$ .

**Instance generation throughput.** Therefore, the generation throughput (tokens per second) for instance  $i$  is the number of running trajectories divided by the per-decoding-step latency, as each step generates one token per trajectory in a batched decode:

$$\mathcal{T}_i = \frac{n_i}{\mathcal{L}_i} = \frac{n_i}{k_1 \times \text{kv\_cache}_i + \max(k_2, k_3 \times n_i) + k_4}. \quad (12)$$

To align with the paper’s notation, we use the snapshot  $S[i]$ , where its field  $S[i].\text{run\_trajs}$  gives the set of running trajectories for instance  $i$ , and thus  $n_i = |S[i].\text{run\_trajs}|$ . The KV Cache memory consumption for the instance is similarly referenced as  $S[i].\text{kv\_cache}$ .

Thus, we obtain the final throughput estimation presented in the paper:

$$\mathcal{T}_i(S) = \frac{|S[i].\text{run\_trajs}|}{k_1 \times S[i].\text{kv\_cache} + \max(k_2, k_3 \times |S[i].\text{run\_trajs}|) + k_4}. \quad (13)$$

The coefficients  $k_1$  through  $k_4$  are determined via offline profiling of the rollout engine and linear regression.

## B.2 Estimation Accuracy

We assess the accuracy of our cost model,  $\mathcal{T}_i(S)$ , by comparing the estimated generation throughput with the actual throughput observed in our experiments. Figure 24 presents the results. The experimental setup aligns with §6.5, using Qwen3-30B-A3B on 128 GPUs, a batch size of 128, a group size of 16, a response length of 40K, and a *staleness bound* of 3. The constant coefficients used in the cost model are profiled and summarized in Table 4.

As shown in the figure, our cost model provides an accurate estimation of the actual throughput, with only a few outliers. The average estimation error is 10.52%, demonstrating that the model can reliably guide the subsequent rollout coordination strategies to tune system throughput.

## C Ablation Study on Redundant Rollout

This section investigates the impact of redundant rollout on system performance. As illustrated in §4.3 and Figure 8(b), redundant rollout involves generating more trajectories than needed for a given batch size or group size, then aborting the excess once the batch or group is full. This technique helps filter out excessively long or time-consuming trajectories, reducing data skewness and improving overall system throughput.

We use the same experimental setup as in §6.5: Qwen3-30B-A3B on 128 GPUs, with a batch size of 128, group size of 16, response length of 40K, and a *staleness bound* of 3. To quantify the redundancy, we define the *redundant ratio*, which specifies the fraction of extra trajectories generated beyond the required number for training. For example, with a *redundant ratio* of 1/16, for a batch size of 128 and a group size of 16, batch-level redundant rollout generates  $128 + 128/16 = 136$  trajectory groups per step, while group-level

redundant rollout generates  $16 + 16/16 = 17$  trajectories per group. In both cases, the total number of trajectories per step increases to  $128 \times 16 \times (1 + 1/16) = 2176$ .

Figure 25 illustrates the effects of batch-level and group-level redundant rollout with a *redundant ratio* of 1/16. We observe a noticeable reduction in both the mean and maximum response lengths per step, with a more significant effect when using batch-level redundancy. This occurs because trajectories within a group tend to be either all long or all short; although the *redundant ratio* is the same, batch-level redundancy exerts a stronger impact as it may discard an entire group consisting of long sequences.

Due to the overall shortening of sequences, the number of tokens processed per step decreases, leading to a clear reduction in post-training time per step. Besides, system throughput, calculated as the total number of tokens divided by the total time, improves modestly. Although both total tokens and total time decrease, redundant rollout helps eliminate excessively long trajectories, thereby reducing overall data skewness and thus improving throughput.

The experiments in §6 do not employ this technique because, as we observed, it introduces a noticeable distribution shift in the generated length. To ensure a fair comparison with the baselines, we choose to discuss it separately here as an ablation study.

## D Detailed Algorithms for Rollout Coordination Strategies

In this section, we present the detailed algorithms for all rollout coordination strategies introduced in §5.3: the *routing strategy* (Algorithm 3), the *synchronization strategy* (Algorithm 4), and the *migration strategy* (Algorithm 5). These strategies rely on a helper function that determines whether a given trajectory  $\tau$  can be assigned to a specific rollout instance  $i$  without violating the staleness constraint. This function is implemented as shown in Algorithm 2. Collectively, these algorithms enable staleness-aware, throughput-oriented rollout coordination, effectively mitigating data skewness and enhancing overall system performance.

### Algorithm 2: Check routable.

---

**Input:**  $S$ : snapshot,  $\tau$ : trajectory to be routed,  $i$ : target instance  
**Output:** Boolean indicating if trajectory  $\tau$  can be routed to instance  $i$  without violating the staleness constraint

```

1 if  $\tau.V_{traj} = \text{None}$  then
2   |    $\tau.V_{traj} \leftarrow S[i].inst\_version$  ;
3   |   if staleness_manager_verify( $\tau.V_{traj}$ ) then
4   |     |   return True ;
5 else
6   |   if  $S[i].inst\_version \geq \tau.V_{traj}$  then
7   |     |   return True ;
8 return False ;

```

---

### Algorithm 3: Routing strategy.

---

**Input:**  $S$ : snapshot of rollout instances,  $ts\_trajs$ : trajectories in TS  
**Output:** List of (instance, trajectories) pairs for routing

```

1 routing  $\leftarrow \emptyset$  ; // Routing list
2 MLQ  $\leftarrow \text{sort}(ts\_trajs)$  ; // Order by  $V_{traj}$  ascending
3 stop  $\leftarrow \text{False}$  ; // Signal to stop
4 foreach  $queue \in MLQ$  do
  | // Skip lower-priority queues if higher ones exist
5   if  $stop$  then
6     |   break ;
7   while  $queue$  is not empty do
8     |    $t \leftarrow queue.\text{peek}()$  ; // Peek at the front trajectory
9     |   // Step 1: Find all candidate instances
10    |   candidates  $\leftarrow \emptyset$  ;
11    |   foreach  $instance i \in S$  do
12      |     |   if check_routable( $S, \tau, i$ ) then
13      |       |       candidates  $\leftarrow candidates \cup \{i\}$  ;
14    |   if  $candidates = \emptyset$  then
15      |     |   stop  $\leftarrow \text{True}$  ;
16      |     |   break ;
17    |   // Step 2: Group candidates by instance model
18    |   |   version (ascending)
19    |   groups  $\leftarrow \text{group\_by\_ascending\_version}(candidates, S)$  ;
20    |   // Step 3: Compute ideal throughput gain
21    |    $\Delta\mathcal{T}_{ideal} \leftarrow \frac{1}{k_1 \times k_2 \times \tau.length + \max(k_2, k_3) + k_4}$  ;
22    |   // Step 4: Waterfall model selection
23    |   selected  $\leftarrow \text{None}$  ;
24    |   foreach  $group \in groups$  do
25      |     |    $\Delta\mathcal{T}_{max} \leftarrow -\infty$  ;
26      |     |   best_inst  $\leftarrow \text{None}$  ;
27      |     |   foreach  $instance i \in group$  do
28        |       |        $\Delta\mathcal{T}_i \leftarrow \text{compute\_marginal\_gain}(S, \tau, i)$  ;
29        |       |       if  $\Delta\mathcal{T}_i > \Delta\mathcal{T}_{max}$  then
30          |         |         |    $\Delta\mathcal{T}_{max} \leftarrow \Delta\mathcal{T}_i$  ;
31          |         |         |   best_inst  $\leftarrow i$  ;
32        |       |       if  $\Delta\mathcal{T}_{max} \geq \mu \times \Delta\mathcal{T}_{ideal}$  then
33          |         |         selected  $\leftarrow best\_inst$  ;
34          |         |         break ; // Accept (above the threshold)
35      |     |   if  $selected \neq \text{None}$  then
36        |       |       // Step 5: Route trajectory
37        |       |       routing.append((selected,  $\{\tau\}$ )) ;
38        |       |       queue.pop() ; // Remove from queue
39        |       |        $S[selected] \leftarrow \text{update\_snapshot}(S[selected], \tau)$  ;
40      |     |   else
41        |       |       stop  $\leftarrow \text{True}$  ;
42        |       |       break ; // No instance meets threshold
43    |   return routing ;

```

---

---

**Algorithm 4:** Synchronization strategy.

---

**Input:**  $S$ : snapshot of rollout instances,  $ts\_trajs$ : trajectories in TS,  $ps\_version$ : current PS model version

**Output:** List of instances for synchronization

```
1 sync ←  $\emptyset$ ; // Instances to synchronize
2 candidates ←  $\emptyset$ ; // Candidate instances to synchronize
// Step 1: Identify eligible instances
3 foreach instance  $i \in S$  do
4   if  $ps\_version > S[i].inst\_version$  then
    // Check if any trajectory can be routed to
    // instance  $i$  under the current version
    can_route ← False;
    foreach trajectory  $\tau \in ts\_trajs$  do
      if  $check\_routable(S, \tau, i)$  then
        can_route ← True;
        break;
    if not can_route then
      candidates ← candidates  $\cup \{i\}$ ;
    // Step 2: Tentative update for each candidate
12 foreach instance  $i \in candidates$  do
  // Create tentative snapshot with updated version
   $S_{temp} \leftarrow S$ ;
   $S_{temp}[i].inst\_version \leftarrow ps\_version$ ;
  // Simulate routing on the tentative snapshot
  routing ← RoutingStrategy( $S_{temp}, ts\_trajs$ );
  // Check if any trajectory would be routed to this
  // instance
  routed_to_i ← False;
  foreach  $(inst, trajs) \in routing$  do
    if  $inst = i$  then
      routed_to_i ← True;
      break;
  if routed_to_i then
    sync.append( $i$ );
23 return sync;
```

---

---

**Algorithm 5:** Migration strategy.

---

**Input:**  $S$ : snapshot of rollout instances

**Output:** List of (instance, trajectories) pairs for migration

```
1 migration ←  $\emptyset$ ; // Migration list
// Case 1: Handle instances with excessive waiting
// trajectories
2 foreach instance  $i \in S$  do
3   wait_cnt ←  $|S[i].wait\_trajs|$ ;
4   if  $wait\_cnt > \varphi_{wait}$  then
5     excess ← wait_cnt  $- \varphi_{wait}$ ;
6     mig_trajs ← excess trajectories from  $S[i].wait\_trajs$ ;
7     migration.append(( $i, mig\_trajs$ ));
8      $S[i].wait\_trajs \leftarrow S[i].wait\_trajs \setminus mig\_trajs$ ;
// Case 2: Handle excessive throughput imbalance
// between instances
9 throughputs ←  $\emptyset$ ;
10 foreach instance  $i \in S$  do
11   throughputs[ $i$ ] ←  $\mathcal{T}_i(S)$ ; // Compute throughput using
    // cost model
12 max_inst ←  $\arg \max_i$  throughputs[ $i$ ];
13 min_inst ←  $\arg \min_i$  throughputs[ $i$ ];
14 gap ←  $\frac{throughputs[max\_inst]}{throughputs[min\_inst]}$ ;
15 if gap  $> \varphi_{throughput}$  then
16   all_trajs ←  $S[max\_inst].run\_trajs \cup S[max\_inst].wait\_trajs$ ;
   // Remove trajectories already handled in Case 1
17   foreach  $(mig\_inst, mig\_trajs) \in migration$  do
18     if  $mig\_inst = max\_inst$  then
19       all_trajs ← all_trajs  $\setminus mig\_trajs$ ;
20   if all_trajs  $\neq \emptyset$  then
21     migration.append((max_inst, all_trajs));
22 return migration;
```

---